Composition and evolution of the lithospheric mantle in central Spain: inferences from peridotite xenoliths from the Cenozoic Calatrava volcanic field

C. VILLASECA[1]*, E. ANCOCHEA[1], D. OREJANA[1] & T. E. JEFFRIES[2]

[1]*Departamento de Petrología y Geoquímica, UCM-CSIC, Facultad de Geología, c/Jose Antonio Novais, 2, 28040 Madrid, Spain*

[2]*Department of Mineralogy, Natural History Museum, London SW7 5BD, UK*

**Corresponding author (e-mail: granito@geo.ucm.es)*

Abstract: Spinel lherzolite xenoliths from the Cenozoic Calatrava volcanic field provide a sampling of the lithospheric mantle of central Spain. The xenoliths are estimated to originate from depths of 35–50 km. Trace element content of clinopyroxene and Cr-number in spinel indicate low degrees of partial melting (≤5%) of the xenoliths. Although a major element whole-rock model suggests wider degrees of melting, the Calatrava peridotite chemistry indicates a moderately fertile mantle beneath central Spain. Calatrava peridotite xenoliths bear evidence for interaction with two different metasomatic agents. The enrichment in LREE (light rare earth element), Th, U and Pb, and the negative anomalies in Nb–Ta in clinopyroxene and amphibole from xenoliths of El Aprisco, indicate that the metasomatic agent was probably a subduction-related melt, whereas the enrichment in MREE in clinopyroxene from xenoliths of the Cerro Pelado centre suggests an alkaline melt similar to the host undersaturated magmas. These metasomatic agents are also consistent with the chemistry of interstitial glasses found in xenoliths of the two volcanic centres. Differences in metasomatism but also in mantle composition is supported by Sr–Nd whole-rock data, which show a more radiogenic nature for Sr isotopes of samples from the El Aprisco centre ($^{87}Sr/^{86}Sr$ ratios of 0.7035–0.7044 instead of 0.7032–0.7037 for samples from Cerro Pelado). The timing of the subduction-related metasomatic stage is unconstrained, although the Calatrava intraplate volcanism intrudes an old Variscan lithospheric section reworked during the converging plate system affecting SE Iberia in the Tertiary. The presence of wehrlite types within the Calatrava peridotite xenoliths is here interpreted as a reaction of host lherzolites with silica-undersaturated silicate melts that could be related to the Calatrava alkaline magmatism. The Sr–Nd isotopic composition of Calatrava peridotites plot within the European asthenospheric reservoir (EAR) mantle, these values represent more enriched signatures than those found in the other Spanish Cenozoic alkaline province of Olot.

Studies of ultramafic xenoliths exhumed by Cenozoic volcanic activity have provided substantial information regarding the nature of the subcontinental lithospheric mantle (e.g. Nixon 1987; Downes 2001). In the Iberian peninsula three main Cenozoic volcanic fields have provided significant mantle-derived xenolith suites since studies from the last century: SE Spain (Ossan 1889), Olot (San Miguel de la Cámara 1936) and Calatrava (Ancochea & Nixon 1987) (Fig. 1). Scarce ultramafic xenoliths have also been described in the Cofrentes volcanic area (Ancochea & Nixon 1987; Seghedi *et al.* 2002), and mantle-derived xenoliths have been found in Upper Permian subvolcanic dykes of the Spanish Central System, although they represent mafic–ultramafic cumulates instead of real mantle peridotitic fragments (Orejana *et al.* 2006; Villaseca *et al.* 2007; Orejana & Villaseca 2008).

In this work we study the chemical composition of the Calatrava sample suite, including major and trace elements for the constituent minerals, and major, trace elements and Nd and Sr isotopes for whole rocks. As for many spinel lherzolite xenolith suites, our data indicate the decoupling of chemical features caused by melt extraction during partial melting and subsequent metasomatism. This study, together with that of Bianchini *et al.* (2010), are the first attempts to characterize the subcontinental mantle beneath central Spain.

Geological setting

The Calatrava volcanic field comprises more than 200 volcanic centres in an area of around 5500 km^2 (Ancochea 1982). The volcanic field is exclusively formed by monogenetic edifices,

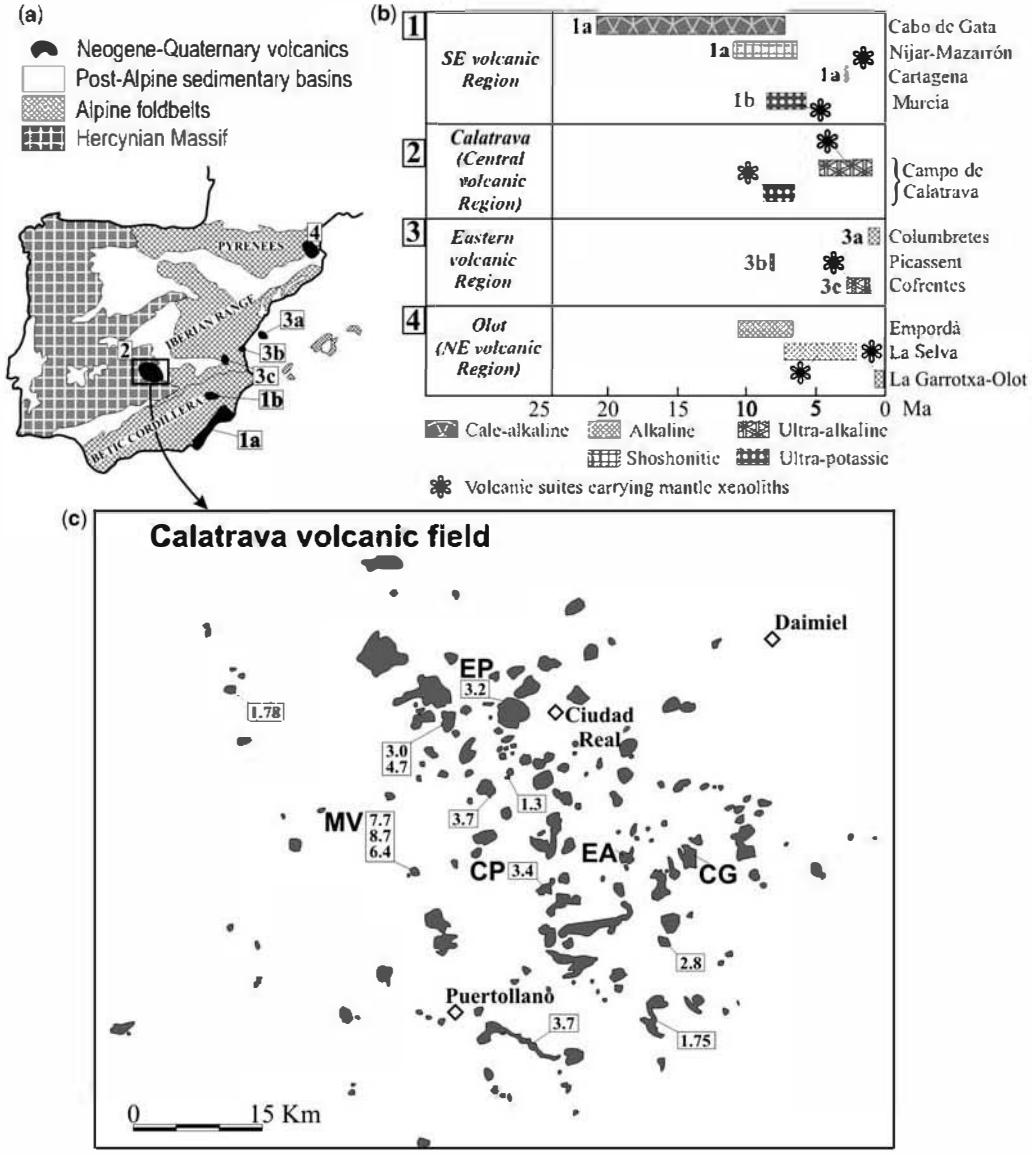

Fig. 1. (a) Sketch map of the Iberian Peninsula showing the location of the Cenozoic volcanic fields. (b) Geochronological table of the different magmatic suites showing those that carry lherzolite xenoliths. (c) Calatrava volcanic field and location of the volcanic centres mentioned in this study: EA, El Aprisco; EP, El Palo (studied by Bianchini *et al.* 2010); CP, Cerro Pelado; CG, Cerro Gordo; MV, Morrón de Villamayor. Numbers inside squares refer to geochronological data (Ancochea 2004).

suggestive of small and short-lived shallow magma chambers. Most edifices are strombolian cones but more than 50 hydromagmatic tuff rings or maars have been also described. Both types of volcanic edifices yield peridotite xenoliths. A first minor ultrapotassic event at around 8.7–6.4 Ma was followed by the eruption of alkaline basalts, basanites, and olivine nephelinites and melilitites from 3.7 to around circa 0.7 Ma (Ancochea 2004). Xenoliths studied in this work have been sampled from the pyroclastic deposits of two undersaturated alkaline basaltic volcanoes: the Cerro Pelado centre (38°48′32″N, 3°54′56″W), an olivine nephelinite scoria cone, and in El Aprisco (38°50′05″N; 3°50′00″W), an olivine melilitite maar. Smaller lherzolite xenoliths appear in other volcanic

centres, including that of the early ultrapotassic event (El Morrón de Villamayor, Cerro Gordo, El Palo, etc.) (Fig. 1), but they have not been sampled for this study.

The similarity in normalized trace element patterns and the Sr–Nd–Pb isotopic homogeneity of the primary alkaline and ultralkaline basic magmas suggest that the Calatrava basaltic suites are derived from different degrees of partial melting of an enriched, but relatively homogeneous mantle source (Ancochea 1982; Cebriá & López-Ruiz 1995). The isotopic composition suggests a HIMU-like reservoir similar to that defined for the European asthenospheric mantle (Granet *et al.* 1995). An enriched asthenospheric reservoir (EAR) is in agreement with the suggested presence of garnet and phlogopite within mantle sources based on trace element geochemistry of Calatrava volcanics (e.g. Ancochea 1982; López-Ruiz *et al.* 2002).

The Calatrava volcanic field is a typical intracontinental zone within the Neogene–Present western and central European province. Similar to the NE Spanish volcanic region (also called the Olot volcanic field), this area is located in the limit of small late Cenozoic sedimentary basins trangressive over Variscan terranes. Volcanic vent distribution does not follow a clear spatial pattern and their geodynamical setting is controversial, with theories invoking a gigantic megafault system affecting the western Mediterranean European block (López-Ruiz *et al.* 2002) or volcanic clustering related to asthenospheric mantle upwelling (hot-spot or diapir instabilities) in a pre-rifting stage (Ancochea 1982; López-Ruiz *et al.* 1993).

Analytical methods

The major element mineral composition has been analysed at the Centro de Microscopía Electrónica 'Luis Bru' (Complutense University of Madrid) using a Jeol JXA-8900 M electron microprobe with four wavelength-dispersive spectrometers. Analytical conditions were an accelerating voltage of 15 kV and an electron beam current of 20 nA, with a beam diameter of 5 μm. Elements were counted for 10 s on the peak and 5 s on each background position. The measurement of Ca in olivine was repeated in some crystals with high content of this element (samples 65290 and 72674) using EMP conditions of 20 kV, 50 nA with counting times of 60 s. To reduce alkali loss during glass analysis, we lowered the beam current to 10 nA and the beam was defocused to 10 μm. Corrections were made using an on-line ZAF method. Detection limits are 0.02 wt% for Al, Na, K and P, 0.03 wt% for Ti, Fe, Mn, Mg, Ni and Cr, and 0.04 wt% for Si.

We have determined the *in situ* concentrations of 30 trace elements (REE, Ba, Rb, Sr, Th, U, Nb, Ta, Pb, Zr, Hf, Y, Sc, V, Co, Zn and Cr) in clinopyroxene (cpx), orthopyroxene (opx), olivine (ol) and amphibole (amph) on >130 μm-thick polished sections using laser ablation (LA-ICP-MS) at the Natural History Museum of London using an Agilent 7500CS ICP-MS coupled to a New Wave UP213 laser source (213 nm frequency-quadrupled Nd–YAG laser). The counting time for one analysis was typically 90 s (40 s measuring gas blank to establish the background and 50 s for the remainder of the analysis). The diameter of the laser beam was around 50 μm. The NIST 612 glass standard was used to calibrate relative element sensitivities for the analyses of the silicate minerals. Each analysis was normalized to Ca or Si (Al for spinel) using concentrations determined by electron microprobe. Detection limits for each element were in the range of 0.01–0.06 ppm, except for Sc and Cr (0.11 and 0.73 ppm, respectively).

Eleven spinel peridotite xenoliths from two volcanic centres (El Aprisco and Cerro Pelado) were used in this investigation. The whole-rock major and trace element composition was analysed at ACTLABS. The samples were melted using $LiBO_2$ and dissolved with HNO_3. The solutions were analysed by inductively coupled plasma atomic emission spectrometry (ICP-AES) for major elements, whereas trace elements were determined by ICP mass spectrometry (ICP-MS). Uncertainties in major elements are bracketed between 1 and 3%, except for MnO (5–10%) and P_2O_5 (>10%). The precision of ICP-MS analyses at low concentration levels was evaluated from repeated analyses of the international standards BR, DR-N, UB-N, AN-G and GH. The precision for Rb, Sr, Zr, Y, V, Hf and most of the REE were in the range 1–5%, whereas they range from 5 to 10% for the rest of trace elements, including Tm. Some samples had concentrations of certain elements below detection limits (K_2O 0.01%; Rb 1; Zr 1; Nb 0.2; Tb 0.01; Ho 0.01; Tm 0.005; Lu 0.002; Hf 0.1; Ta 0.01; Th 0.05; U 0.01). More information on the procedure, precision and accuracy of ACTLABS ICP-MS analyses is available at www.actlabs.com.

Sr–Nd isotopic analyses were carried out at the CAI de Geocronología y Geoquímica Isotópica of the Complutense University of Madrid, using an automated VG Sector 54 multicollector thermal ionization mass spectrometer with data acquired in multidynamic mode. Isotopic ratios of Sr and Nd were measured on a subset of whole-rock powders. The analytical procedures used in this laboratory have been described elsewhere (Reyes *et al.* 1997). Repeated analysis of NBS 987 gave $^{87}Sr/^{86}Sr = 0.710249 \pm 30$ (2σ, $n = 15$) and

for the JM Nd standard the $^{143}Nd/^{144}Nd = 0.511809 \pm 20$ (2σ, $n = 13$). The 2σ error on the ε(Nd) calculation is ± 0.4.

Petrography and mineral chemistry

The studied Calatrava mantle xenoliths are rounded medium-size samples (from 5 to 45 cm in diameter) that show no evidence of alteration or host basalt infiltration. Xenoliths equilibrated in the spinel peridotite stability field and display a wide modal variation from lherzolite to minor wehrlite types. Modal composition was determined by mass-balance calculations from the main minerals and the major element compositions of the whole rocks, using the least-squares inversion method of Albarède (1995). Within the 11 analysed rock samples, 10 are lherzolites and only one is a wehrlite (sample 72674) (Fig. 2). Mantle xenoliths from the El Aprisco centre tend to have orthopyroxene more abundant than clinopyroxene, whereas those from Cerro Pelado are more clinopyroxene-rich, even wehrlitic in composition (Fig. 2). The lherzolitic–harzburgitic mantle xenoliths from Olot (Bianchini *et al.* 2007; Galán *et al.* 2008) have been plotted for comparison, and are similar in modal composition to those from SE Spain (Tallante: Beccaluva *et al.* 2004) (not shown). Calatrava lherzolites are richer in clinopyroxene and poorer in olivine than other Spanish mantle xenolith suites (Fig. 2). Scarce phlogopite-rich clinopyroxenites (glimmerite varieties) have been found at Cerro Pelado (Ancochea & Nixon 1987) but they have not been sampled for this study.

Although in accessory amounts, the studied peridotite xenoliths usually have interstitial volatile-rich phases indicative of modal metasomatism: amphibole in samples from the El Aprisco centre, and phlogopite from those of the Cerro Pelado maar. Only one xenolith is an anhydrous lherzolite (sample 72690 from El Aprisco). The wehrlite 72674 shows trace amounts of phlogopite included in clinopyroxene. Although peridotite xenoliths from Cerro Pelado with both hydrous minerals, amphibole and phlogopite, have been described previously (Ancochea & Nixon 1987) we did not find this type.

Most peridotite xenoliths have a coarse-grained texture of protogranular aspect, defined by a grain size greater than 2 mm and commonly equigranular (Fig. 3a). Some porphyroclastic textures or more inequigranular varieties also appear, in which olivine or orthopyroxene are commonly the porphyroclasts. Grain boundaries are usually curvilinear defining mosaic or triple-junction textures. No phase layering, foliation or lamination have been found.

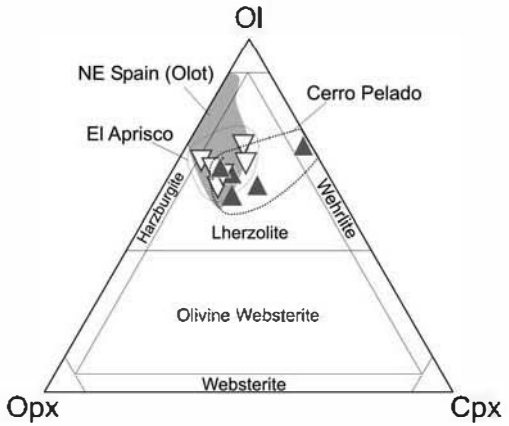

Fig. 2. Modal proportions of the studied Calatrava mantle xenoliths calculated using the mass-balance method of Albarède (1995). The modal compositional field from mantle xenoliths from NE Spain (Olot) is taken from Bianchini *et al.* (2007) and Galán *et al.* (2008).

Olivine crystals may have different sizes even in a single sample. Some fine-grained interstitial crystals, spatially related to spinel microaggregates or spinel coronas as described below, have been considered to be of second generation. Both orthopyroxene and clinopyroxene show mutual lamellae, and commonly a second superimposed spinellamellae. Spinel occurs as discrete, dispersed interstitial grains that usually show some fine-grained polycrystalline coronas of amphibole (only in the El Aprisco outcrop) (Fig. 3b–d). Some scarce spinel–pyroxene–amphibole symplectite has been also observed, but the clearly hydrous character of the corona rejects the possibility of a reaction between pre-existing garnet and matrix olivine, as suggested in other spinel symplectitic lherzolite xenoliths (Ackerman *et al.* 2007) (Fig. 3c). Some spinel grains have sieve textures defined by a partial corona of a new fine-grained spinel-2 associated to vesicular glass and second-generation olivine (Fig. 3f). These textural features have been interpreted as re-equilibrations or reactions with a

Fig. 3. Photomicrographs of representative Calatrava mantle xenoliths. *Lherzolite 72691* (El Aprisco): (a) equigranular texture; (b) interstitial amphibole around major peridotite minerals (spinel, clinopyroxene, orthopyroxene) (BSE image); and (c) symplectitic intergrowths of spinel-2, amphibole, clinopyroxene-2 (an amph–cpx intergrowth is shown on the left) within orthopyroxene (BSE image). *Lherzolite 72689* (El Aprisco) showing: (d) amphibole aureoles around spinel; and (e) a complex reaction zone showing the breakdown of spinel to clinopyroxene-2, olivine-2 and vesicular

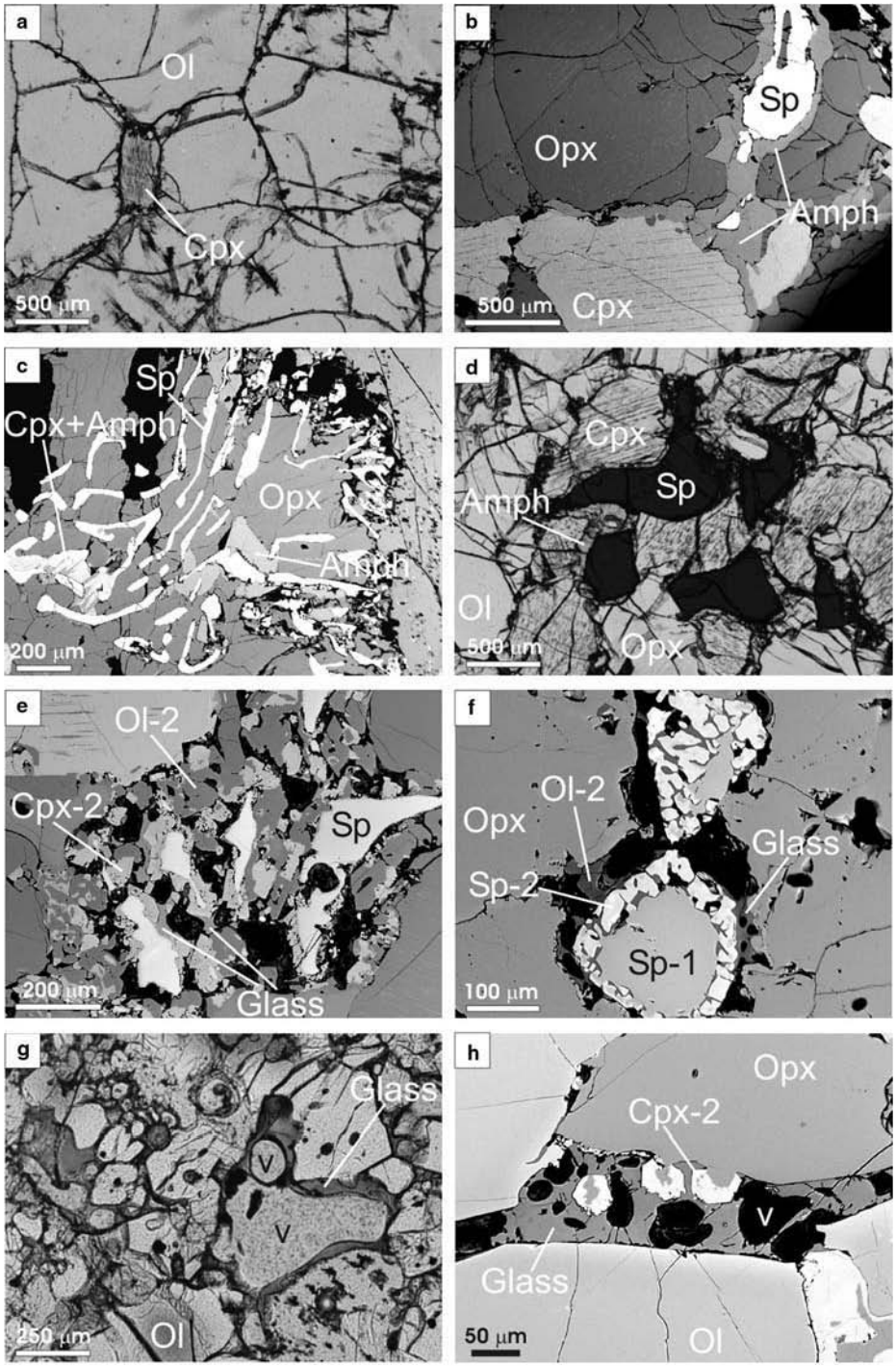

Fig. 3. (*Continued*) glass (BSE image). *Lherzolite 65290* (Cerro Pelado): (**f**) reaction zones around primary spinel (Sp-1) composed of cellular spinel-2, microgranular olivine-2 and vesicular glass (BSE image). *Wehrlite 72674* (Cerro Pelado): (**g**) highly vesicular interstitial glass (BSE image); and (**h**) vesicular glass vein with associated cpx-2 crystals (BSE image). Ol, olivine; Opx, orthopyroxene; Cpx, clinopyroxene; Sp, spinel; Amph, amphibole; v, vesicle.

percolating intergranular melt (Shaw & Dingwell 2008). In sample 65290 it is possible to see a complex corona of symplectitic spinel-2 and interstitial glass rimming primary spinel (Fig. 3f). Acicular pentlandite, interstitial to olivine, is very scarce in some lherzolites.

Accessory amounts of hydrous minerals (amphibole or phlogopite) are present in most of the Calatrava lherzolite xenoliths (except in anhydrous lherzolite 72690). They are mostly intergranular phases forming small anhedral crystals. Amphibole in most lherzolites forms coronas around spinel grains or intergrowths with clinopyroxene around spinel symplectites (Fig. 3b–d), in textures similar to those described in other peridotite xenolith suites (e.g. Coltorti *et al.* 2004, 2007*b*).

Some xenoliths also show interstitial brown glass with small vesicle or bubble-like structures (Fig. 3e–h). Moreover, some interstitial glasses appear as part of a complex reaction zone that involves many of the primary lherzolite minerals, but especially spinel, which is surrounded either by symplectitic intergrowths of new spinel-2 and olivine-2 with interstitial glass (Fig. 3f) or by a microaggregate of newly formed cpx–ol–glass (Fig. 3e).

The wehrlite 72674 is porphyroclastic in texture and the two pyroxenes do not show lamellar exsolution, as is typical in the lherzolite types. Wehrlite clinopyroxene shows a marked poikilitic texture with multiple glass, apatite, phlogopite and fluid-rich inclusions. Olivine grains show locally deformation twins and most crystals have smooth curvilinear boundaries. Only trace amounts of spinel (as microinclusions in olivine and clinopyroxene) appear in this sample. The wehrlite also shows interstitial vesicular glass, which is mainly concentrated in the fine-grained section of the inequigranular texture, defining some interconnected veining (Fig. 3g, h).

Major element mineral composition

The Calatrava hydrous mantle xenoliths consist of variable proportions of magnesian olivine, orthopyroxene and clinopyroxene, aluminous spinel, and accessory amounts of calcic amphibole or phlogopite, the compositions of which are summarized in Table 1. All minerals are unzoned and homogeneous within a single crystal.

The Mg-number for olivine mostly ranges from 89.2 to 91.5, although neoformed varieties (oliv-2) and olivine from wehrlite 72674 show lower Mg-numbers (88.4 and 84.5–86.0, respectively). Olivine-2 in lherzolites also show slightly higher CaO and lower NiO content than Mg-rich olivine (Table 1), features typical of metasomatism (e.g. Coltorti *et al.* 1999; Ionov *et al.* 2005). Olivine in the wehrlite shows the highest TiO_2 content (up to 0.09 wt%), and high CaO and low NiO content (Table 1).

Orthopyroxene has a similar range of Mg-numbers than olivine, mostly from 88.7 to 92.3 (Table 1), but it shows a wider range in content of Cr_2O_3 (0.13–0.52), Al_2O_3 (3.00–5.74) and CaO (0.12–1.09), always in a common range for abyssal peridotites (Bonatti & Michael 1989). Correlatively to olivine, orthopyroxene of wehrlite 72674 shows lower Mg-numbers (85.0–86.6), and higher content of TiO_2 (0.22–0.41), CaO (0.94–3.86) and Na_2O (0.12–0.25), than orthopyroxene from associated lherzolites (Fig. 4a). Lherzolite 72691 with the lowest averaged Al content of orthopyroxene (and the highest Mg-Cr values) could be the most depleted peridotite of the xenolith suite (Fig. 4a).

Clinopyroxene also shows a wide range of Mg-numbers (87.6–92.7) with cpx-2 (neocrystals related to intergranular reaction zones) having low values (88.2–90.0) but variable Al–Ti–Cr content. For example, the cpx-2 analysis 71 in lherzolite 72689 (related to a spinel reaction zone with glass) shows the highest Al–Cr–Ti content of the whole analysed clinopyroxene population (Fig. 4b). Clinopyroxene from wehrlite 72674 is also Fe–Ti-enriched, as are the other minerals of this xenolith (Fig. 4b, c) (Table 1). Lherzolite 72691 shows the lowest Al clinopyroxene, reinforcing the idea of being the most depleted peridotite xenolith.

Primary spinel has low Cr-numbers (from 8.3 to 10.8) and a narrow Mg-number range (0.75–0.78) (Table 1). TiO_2 content is generally low, ranging from 0.01 to 0.16 wt%. Spinel from the most depleted lherzolites (samples 72691 and 55570) shows a wider range of composition, with relatively higher Cr values and lower Al content than spinel from associated lherzolites (Fig. 5). In lherzolite 55570 cores of large spinel crystals show the highest Al and Mg content (and the lowest Cr values) compared with rims or interstitial rods, which are associated with intergranular amphibole. In fact, the smallest interstitial spinel crystals in lherzolite 55570 and the symplectitic spinel from lherzolite 72691 show the highest Cr-numbers (13.0–17.7) and the lowest Al_2O_3 contents (51–55 wt%) of the Calatrava lherzolites. These contents are similar to those of the sieved sp-2 of lherzolites 65290 and 65298, which also show high TiO_2 content (up to 0.44 wt%), suggestive of a reaction with a Ti-rich metasomatic agent (Perinelli *et al.* 2008*b*) (Fig. 5). Residual spinel micrograins preserved as inclusions in major minerals of wehrlite 72674 show the highest Ti and Cr (TiO_2 up to 3.0 wt% and Cr-numbers in the range of 52.4–54.1), and the lowest Al–Mg content, of the studied peridotite xenoliths (Table 1). Owing to

Table 1. *Major element composition of representative minerals from the Calatrava mantle xenoliths*

Representative olivines

	El Aprisco						Cerro Pelado			
Sample	55569 A39	55570 A18	72688 A142	72689 A82	72690 A38	72691 A120	65290 A23	65298 A2	65298 21 (oliv-2)	72674 A95
SiO_2	41.33	40.56	41.05	39.97	41.20	40.63	40.58	40.67	40.69	40.03
TiO_2	bdl	bdl	bdl	bdl	0.01	bdl	0.02	0.01	0.01	0.03
Al_2O_3	bdl	bdl	0.02	bdl	bdl	bdl	0.03	bdl	bdl	bdl
FeO	9.63	9.18	9.88	9.53	9.31	8.66	10.40	9.29	11.36	14.85
MnO	0.15	0.18	0.20	0.18	0.06	0.13	0.16	0.07	0.13	0.12
MgO	49.60	49.54	49.61	49.85	49.74	50.68	49.01	50.43	48.71	45.53
CaO	0.03	0.04	0.09	0.04	0.02	0.05	0.06	0.09	0.13	0.09
Na_2O	bdl	0.02	0.01	bdl	0.02	0.01	bdl	0.01	bdl	bdl
K_2O	0.01	bdl	bdl	bdl	bdl	bdl	bdl	bdl	bdl	bdl
NiO	0.41	0.47	0.22	0.42	0.33	0.42	0.21	0.36	0.12	0.20
Cr_2O_3	bdl	0.08	0.01	0.07	0.02	0.03	0.07	0.03	0.04	bdl
Total	101.06	99.98	101.09	99.99	100.71	100.58	100.49	100.92	101.15	100.91
XMg	90.19	90.59	89.97	90.31	90.50	91.25	89.36	90.62	88.44	84.47

Representative orthopyroxenes

	El Aprisco						Cerro Pelado			
Sample	55569 A36	55570 A32	72688 A59	72689 A76	72690 A41	72691 A65	65290 A27	65298 A23	65298 A3	72674 A110
SiO_2	55.08	54.47	55.38	54.97	54.73	54.71	54.19	54.24	53.88	53.64
TiO_2	0.15	0.12	0.03	0.06	0.04	0.04	0.18	0.07	0.08	0.37
Al_2O_3	4.72	5.00	3.49	3.35	5.42	4.08	5.74	5.49	5.39	3.94
FeO	6.26	5.77	6.54	6.41	5.80	5.45	6.30	6.11	6.24	8.46
MnO	0.14	0.14	0.15	0.15	0.12	0.13	0.14	0.15	0.13	0.15
MgO	32.80	32.56	33.39	33.94	32.34	33.66	31.53	32.96	32.81	28.54
CaO	0.99	1.10	0.54	0.43	1.37	0.62	1.04	0.88	0.80	3.86
Na_2O	0.11	0.11	0.02	0.03	0.13	0.06	0.15	0.12	0.15	0.25
K_2O	bdl	bdl	0.02	bdl	bdl	bdl	bdl	bdl	bdl	bdl
NiO	0.08	0.14	bdl	0.08	0.08	0.15	0.04	0.18	0.14	bdl
Cr_2O_3	0.33	0.53	0.18	0.23	0.34	0.38	0.40	0.35	0.33	0.44
Total	100.68	99.93	99.74	99.66	100.38	99.29	99.70	100.55	99.95	99.64
XMg	90.31	90.94	90.11	90.38	88.94	91.66	89.92	90.59	90.35	85.78

(*Continued*)

Table 1. *Continued*

Representative clinopyroxenes

	El Aprisco							Cerro Pelado				
Sample	55569 A30	55570 A30	72688 A57	72689 71 (Cpx-2)	72689 A75	72690 A42	72691 A66	65290 A31	65298 22 (Cpx-2)	65298 A4	72674 101 (Cpx-2)	72674 A96
SiO_2	52.29	51.75	51.89	49.86	51.05	52.37	52.57	51.19	53.03	51.36	53.97	49.49
TiO_2	0.46	0.23	0.42	0.80	0.41	0.33	0.01	0.54	0.51	0.52	0.62	1.39
Al_2O_3	6.90	5.72	4.87	8.11	6.07	7.61	4.44	7.37	4.43	7.11	3.12	6.70
FeO	2.60	2.87	2.86	3.08	2.73	2.46	2.33	3.46	4.21	3.31	6.11	4.80
MnO	0.05	0.06	0.14	0.02	0.10	bdl	0.05	0.09	0.17	0.06	0.16	bdl
MgO	14.94	15.81	15.66	15.65	15.35	14.44	16.64	15.72	17.72	15.66	17.90	14.39
CaO	19.69	21.15	22.26	18.80	21.58	20.55	21.29	18.90	18.17	19.09	16.57	20.95
Na_2O	1.62	1.35	0.87	1.19	0.98	1.64	0.89	1.60	1.21	1.61	1.04	1.04
K_2O	bdl	bdl	bdl	bdl	bdl	0.01	bdl	0.01	bdl	bdl	0.03	bdl
NiO	0.04	0.08	0.03	0.01	0.03	0.07	0.05	bdl	bdl	0.01	0.01	0.01
Cr_2O_3	0.79	0.83	0.54	1.50	0.70	0.94	0.61	0.74	0.97	0.66	0.63	0.59
Total	99.36	99.85	99.55	99.03	98.99	100.42	98.88	99.63	100.41	99.39	100.14	99.34
XMg	91.10	90.79	90.72	90.06	90.98	91.56	92.65	88.98	88.20	89.33	83.94	84.20
XCr	0.07	0.09	0.06	0.08	0.07	0.07	0.10	0.09	0.13	0.06	0.12	0.09

Representative spinels

	El Aprisco							Cerro Pelado				
Sample	55569 A40	55570 A16	72688 A144	72689 A90	72690 A55	72691 121 sympl.	72691 56 sympl.	65290 A29	65290 A30 (Sp-2)	65298 A5 (Sp-2)	65298 A1	72674 A13
SiO_2	0.07	0.02	0.13	0.07	0.06	0.05	0.04	0.08	0.11	0.11	0.08	0.11
TiO_2	0.13	0.10	0.10	0.06	0.10	0.01	bdl	0.19	0.41	0.38	0.14	2.49
Al_2O_3	56.51	52.23	55.96	57.78	58.40	53.85	51.03	56.97	53.15	51.64	56.83	20.76
Cr_2O_3	10.17	15.73	9.61	8.84	10.15	13.10	16.32	10.17	13.11	14.46	9.31	35.80
FeO	11.97	12.09	13.23	12.00	10.57	10.90	11.73	12.55	11.99	11.10	11.15	26.37
MnO	0.04	0.10	0.15	0.11	0.041	0.10	0.07	0.02	0.11	0.13	0.10	0.19
NiO	0.34	0.33	0.29	0.48	0.39	0.40	0.25	0.32	0.34	0.28	0.34	0.11
MgO	20.41	19.65	19.81	20.49	21.12	20.82	19.90	20.23	20.62	20.93	21.56	13.23
CaO	0.03	0.03	0.09	0.01	bdl	0.03	0.06	0.01	0.02	0.03	0.02	0.18
Na_2O	0.04	0.01	0.04	0.01	0.01	bdl	bdl	bdl	bdl	bdl	0.01	bdl
K_2O	bdl	bdl	bdl	bdl	bdl	bdl	bdl	0.01	bdl	bdl	0.02	bdl
Total	100.00	100.28	99.74	100.12	100.84	99.54	99.65	100.78	100.13	99.36	99.93	99.22
XCr	10.78	16.81	10.33	9.30	10.43	14.05	17.66	10.71	14.21	15.83	9.90	53.64
XMg	0.75	0.74	0.73	0.75	0.78	0.77	0.75	0.74	0.76	0.77	0.78	0.48

Representative amphiboles and phlogopites

	Amphibole						Phlogopite		
Sample	55569 A27	55570 A35	72689 A85	72691 A55	72688 A51	72688 A68	65298 A13	65298 A19	72674 A116
SiO_2	43.83	42.65	42.79	43.63	42.19	42.59	37.64	38.13	35.98
TiO_2	1.48	0.58	0.73	0.42	1.33	1.33	3.10	3.12	6.76
Al_2O_3	14.25	15.43	15.05	14.97	15.18	15.09	17.90	18.18	15.70
FeO	3.72	3.82	4.04	3.72	4.40	4.16	4.17	3.88	8.08
MnO	0.04	0.14	0.05	0.09	0.12	0.04	0.05	bdl	0.09
MgO	17.22	17.86	18.09	18.64	17.67	17.54	21.35	20.54	17.66
CaO	11.48	10.74	11.17	10.83	11.76	11.69	0.02	0.05	0.10
Na_2O	3.51	3.75	3.59	3.62	3.50	3.41	0.79	0.76	0.81
K_2O	0.02	0.20	bdl	0.11	0.06	0.07	9.15	9.37	8.91
NiO	0.25	0.10	0.19	0.08	0.07	0.04	bdl	bdl	bdl
Cr_2O_3	0.57	1.39	0.72	1.34	0.73	0.77	0.78	0.81	0.16
Total	95.54	95.17	95.50	96.02	96.20	95.92	94.93	94.83	94.25
XMg	89.18	89.29	88.87	89.93	87.75	88.27	90.14	90.43	79.58
XCr	2.64	5.71	3.10	5.66	3.14	3.30	2.85	2.90	0.69

Interstitial glasses

	El Aprisco		Cerro Pelado					
Sample	72689 A22	72689 A24	65290 A34	65290 A37	72674 A7	72674 A1	72674 A5	72674 A109
SiO_2	57.73	56.79	55.66	54.60	53.29	53.68	58.17	59.74
TiO_2	0.84	0.80	1.02	1.08	1.92	2.36	1.49	1.78
Al_2O_3	22.22	21.87	21.51	21.63	18.87	18.99	16.52	16.69
FeO	2.01	2.25	2.35	1.86	5.17	4.63	3.75	3.43
MnO	bdl	0.03	0.03	0.03	0.08	0.12	0.02	0.07
MgO	3.09	3.48	3.37	2.74	2.25	1.89	1.87	1.82
CaO	6.70	7.07	4.77	4.81	4.19	3.90	2.37	2.30
Na_2O	5.54	5.02	4.36	5.07	6.26	6.06	5.19	3.34
K_2O	0.06	0.03	4.33	4.87	5.27	5.18	5.44	5.17
P_2O_5	0.11	0.08	0.23	0.20	0.35	0.29	0.24	0.20
Cr_2O_3	0.06	0.12	0.37	0.37	0.07	0.04	0.03	0.03
Total	98.42	97.34	98.00	97.24	97.77	97.18	95.10	94.56
XMg	0.73	0.73	0.72	0.72	0.44	0.42	0.47	0.49

Abbreviation: bdl, below detection limits.

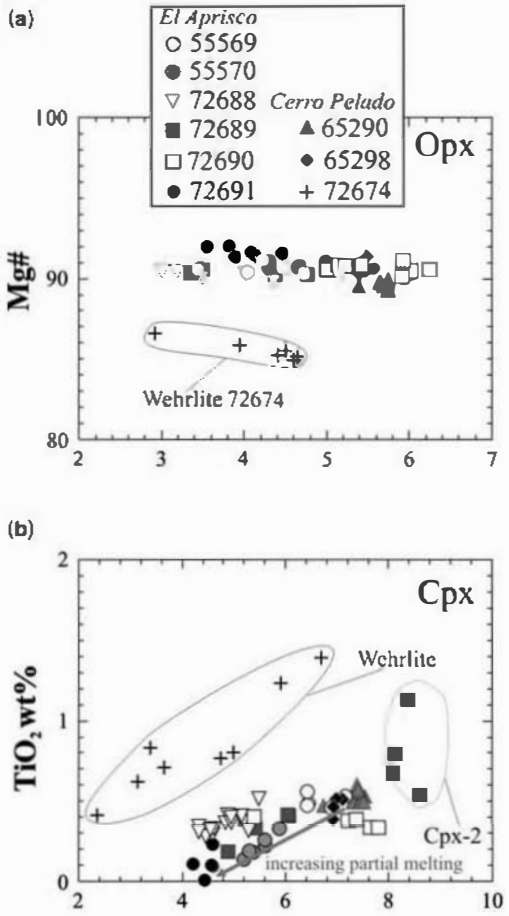

Fig. 4. Major element compositions of pyroxenes in Calatrava peridotite xenoliths. Mg# is the Mg-number. The grey arrow in (b) shows clinopyroxene compositional variation with a progressive increase in peridotite partial melting (Uysal *et al.* 2007).

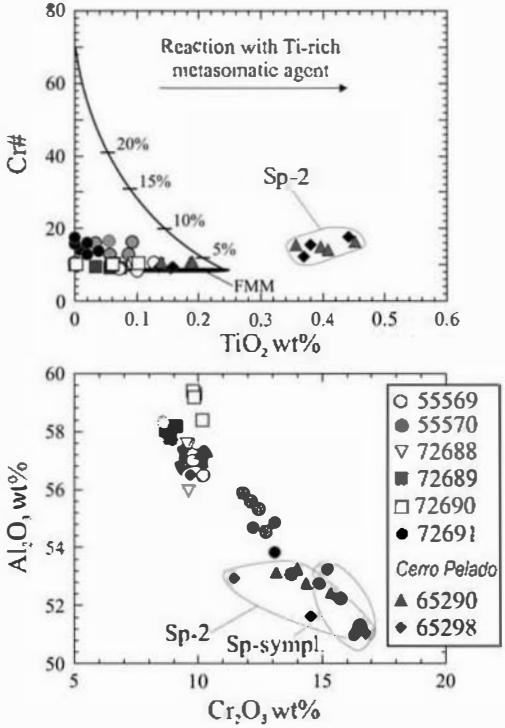

Fig. 5. Composition of spinel from the Calatrava peridotite xenoliths. The trend of partial melting of a fertile MORB mantle (FMM) is shown for comparison. The line of reaction with a metasomatic agent (or a partial melt) is taken from Perinelli *et al.* (2008*b*) and Shaw & Dingwell (2008).

this extreme composition they have not been plotted in Figure 5.

The low Cr-number of primary spinels from the Calatrava lherzolite xenoliths combined with the averaged Mg-number of the coexisting olivine make them plot in the OSMA (olivine–spinel mantle array) closer to fertile mantle compositions (Arai 1992) than other lherzolite xenolith suites from Iberia (Fig. 6). The Cr-spinel of wehrlite 72674 plots outside the OSMA, further to the right of the olot harzburgite field (Fig. 6).

Amphibole is a typical interstitial mineral locally surrounding primary spinel in the lherzolite samples from the El Aprisco maar. Its composition is mainly pargasite. Mg-numbers range from 86.9 to 91.2, and are positively correlated with Cr_2O_3 content (0.7–1.4 wt%) but inversely with TiO_2 (1.48–0.69 wt%) and CaO (11.9–11.0 wt%) content. Amphibole in lherzolites 72691 and 55570 shows the highest Mg- and Cr-numbers (89.3–91.2 and 4.8–5.7, respectively), and the lowest TiO_2 and CaO content (0.3–0.6 and 10.4–10.8 wt%,

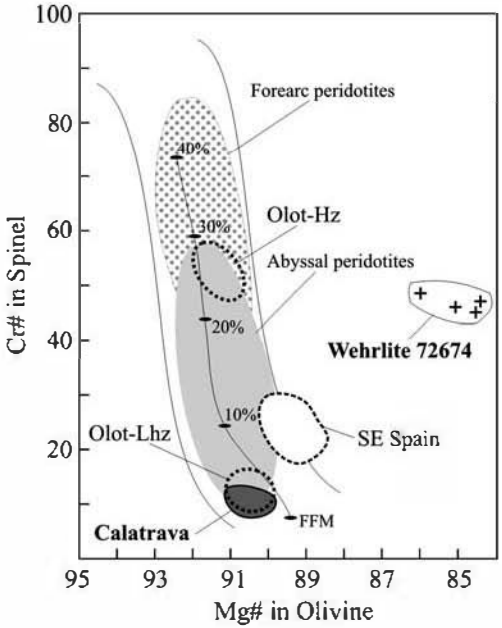

Fig. 6. Cr-number ($100 \times Cr/(Cr + Al)$) in spinel v. Mg-number in coexisting olivine for Iberian mantle xenoliths. Mineral data from the Olot volcanic field (Lhz, lherzolites; Hz, harzburgites) are taken from Bianchini *et al.* (2007) and Galán *et al.* (2008). Data from the SE Spain volcanic field (mainly from the Tallante volcanic centre) are from Beccaluva *et al.* (2004) and Shimizu *et al.* (2004). OSMA–olivine–spinel mantle array (Arai 1994). FMM: fertile MORB mantle and partial melting trends are from Arai (1992). Fields of forearc and abyssal peridotites are from Pearce *et al.* (2000).

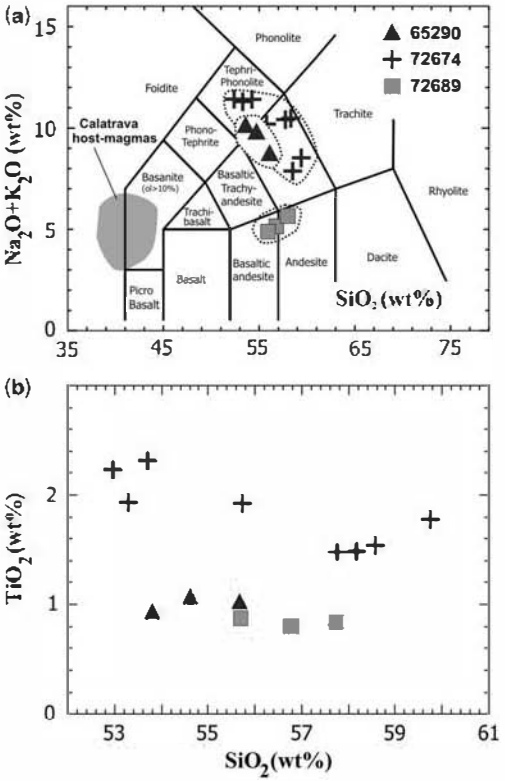

Fig. 7. Chemistry of glasses from Calatrava peridotite xenoliths. (a) The total alkali–silica (TAS) diagram of Le Bas *et al.* (1986) for glasses in Calatrava mantle xenoliths. The grey field for Calatrava volcanic rocks is taken from Ancochea (2004). (b) TiO_2–silica (in wt%) diagram.

respectively). The low-K content of Calatrava amphiboles (<0.11 wt%) is remarkable compared to other mantle xenolith suites (Coltorti *et al.* 2007*a*), except those from some Olot lherzolites (OLT-21 and OLT-23 samples: Bianchini *et al.* 2007).

Phlogopite is only found in mantle xenoliths from the Cerro Pelado centre with Mg-number (90.2–90.4) similar to coexisting clinopyroxene but with higher Cr-number (2.8–2.9) (Table 1). Phlogopite included in clinopyroxene from wehrlite 72674 is markedly poorer in Cr and Mg values (0.7 and 79.6, respectively) but richer in TiO_2 content (6.8 wt%), similar in composition to phlogopites from associated glimmerite xenoliths (anal. 6 in table 32 of Ancochea & Nixon 1987).

Glass veins and interstitial glasses have been observed in some Calatrava mantle xenoliths. In xenoliths from the Cerro Pelado centre the glasses are alkaline in composition and they plot mostly in the field of trachy-andesite in the total alkalis–silica (TAS) diagram (Fig. 7). However, interstitial glass from lherzolite 72689 from the El Aprisco volcano is subalkaline in composition owing to its low K_2O content (Table 1), and plots mostly in the field of basaltic andesite in the TAS diagram. The Calatrava glasses are compositionally heterogeneous, and thus, the high TiO_2 and FeO (and low Al_2O_3 and MgO) content shown by glasses from wehrlite 72674 (1.8–2.3 and 3.3–5.8 wt%, respectively) (Table 1) are quite remarkable (Fig. 7).

Pressure–temperature P–T *estimates*

The lithospheric thickness in central Spain seems to be almost constant over a large area at around 110 km, while the depth to the Moho is around 32 ± 2 km (Fernàndez *et al.* 1998). The depth of xenolith extraction is constrained to less than 70 km (*c.* 20 kbar) by the absence of garnet in the lherzolite suite. Although for spinel peridotites there are no precise geobarometers (e.g. Pearson *et al.* 2005; Ackerman *et al.* 2007), we have used

Table 2. *P–T estimates on the Calatrava mantle xenoliths*

	T (°C)			P (kbar)
	T_{WB}	T_{BM}	T_{BK}	P_{NU}
El Aprisco xenoliths				
55569 cpx30opx36	1093	1185	1052	14.6
55570 cpx30opx32	1116	1220	1073	9.7
72688 cpx57opx59	1003	1036	866	6.4
72689 cpx75opx76	1054	1109	938	8.9
(cpx-2)71opx76	1182	1345	1163	13.9
72690 cpx42opx41	1079	1062	980	15.0
72691 cpx66opx65	1115	1274	994	7.6
Cerro Pelado xenoliths				
65290 cpx31opx27	1149	1382	1112	13.4
65298 cpx4opx3	1165	1321	1123	13.8
(cpx-2)22opx23	1255	1420	1209	7.0
72674 cpx96opx108	1056	1050	986	7.6
(cpx-2)101opx110	1243	1500	1207	7.0

the estimations of Nimis & Ulmer (1998) for clinopyroxene in order to approximate the depth of extraction of the lherzolite xenoliths (Table 2). Pressure estimates range from 14–15 kbar, for weakly metasomatized lherzolites (e.g. anydrous lherzolite 72690, Table 2), to 7–8 kbar for the most depleted lherzolites (72691) or wehrlite varieties (72674). These low-pressure values are unrealistic for mantle depths but suggest that xenoliths could have been trapped from a shallow lithospheric mantle close to Moho depths. The second generation of clinopyroxene, related either to glass veining in lherzolite 72689 (cpx 71, Table 2) or to microaggregates around spinel in lherzolite 65298 (cpx 22, Table 2), yields P estimates mostly overlapping those from primary clinopyroxene (13.9–7.0 kbar). These unrealistic low-pressure estimates are also in disagreement with the absence of replacement of spinel by plagioclase in the studied samples.

Temperatures were calculated using three calibrations of the two-pyroxene geothermometer (Wood & Banno 1973; Bertrand & Mercier 1985; Brey & Köhler 1990). In general there is a good agreement between the different methods used, although Bertrand & Mercier's (1985) temperatures are slightly higher than the two other estimates (Table 2). Most lherzolites yield T estimates in the range of 1000–1165 °C, whereas neoformed clinopyroxene give a still higher temperature range of 1180–1255 °C. We have to bear in mind that most of the neoformed clinopyroxene is related to interstitial glass (e.g. cpx 71 in lherzolite 72689 and cpx 101 in wehrlite 72674, Table 2). Thus, geothermometry suggests some kind of reheating at depth to explain the thermal increase (*c.* 100 °C). The xenolith reaction with high-temperature magmas (e.g. silica-undersaturated alkaline magmas have liquidus temperatures of around 1250–1300 °C: Perinelli *et al.* 2008*a*) may explain the higher temperature of the second-generation clinopyroxene in the Calatrava peridotites.

Trace element mineral composition

Trace element analyses of representative main minerals from two lherzolites are reported in Table 3. REE primitive mantle-normalized patterns for clinopyroxene of amphibole-lherzolite (72688 from the El Aprisco centre) are LREE-enriched ($La_N/Sm_N = 10.4–13.7$) and almost flat in HREE (Fig. 8). The coexisting orthopyroxene displays a similar trend in some LREE patterns (although showing an inflection to Nd instead of Sm as in cpx patterns) but are positively fractionated in HREE (Fig. 8). Olivine shows a similar REE pattern to orthopyroxene, although more spiky and less HREE enriched (not shown, Table 3). Similarly, multitrace element patterns normalized to primitive mantle for clinopyroxene show a marked Th–U enrichment, and Nb–Ta and, to a lesser extent, Zr–Ti negative anomalies (Fig. 8). Coexisting orthopyroxene and, less markedly, olivine show similar trace element patterns.

Amphibole REE patterns perfectly mimic those of the coexisting clinopyroxene (Fig. 8). Incompatible element patterns are also similar to those of clinopyroxene but with higher LILE (large ion lithophile elements) and Ti content. The high Th–U content of amphibole and associated clinopyroxene suggests an enrichment process related to melt instead of a volatile-rich fluid as the metasomatizing agent (see also Coltorti *et al.* 2007*b*). This marked Th–U positive anomaly highlights the prominent Nb–Ta negative anomaly of the El Aprisco

Table 3. *Trace element composition of minerals from the Calatrava lherzolite xenoliths*

	72688 (El Aprisco)						65290 (Cerro Pelado)		
	ol ($n = 4$)	cpx ($n = 12$)	cpx-2 ($n = 3$)	opx ($n = 4$)	amph ($n = 21$)	sp ($n = 2$)	ol ($n = 9$)	cpx ($n = 24$)	opx ($n = 12$)
Sc	6.783	77.70	76.43	23.88	66.59	0.279	6.542	62.83	27.89
V	16.62	202	199	86.83	331	351	5.470	187	98.93
Cr	457	3803	4117	1840	4568	47750	128	4235	2868
Co	116	18.70	19.00	54.35	32.87	187	139	19.44	57.45
Zn	37.88	14.60	15.26	28.38	11.46	885	78.99	11.70	46.71
Rb	0.059	0.048	0.051	0.053	3.377	0.084	0.064	0.048	0.052
Sr	0.180	172	168	0.935	529	0.054	0.060	146	0.803
Y	0.214	18.63	18.467	1.137	33.629	0.023	0.113	24.26	2.320
Zr	0.138	11.36	11.30	0.632	12.13	0.074	0.227	119	12.94
Nb	0.017	0.014	0.015	0.014	0.154	0.094	0.025	1.118	0.082
Ba	0.281	2.862	0.189	0.142	845	0.084	0.142	0.089	0.086
Hf	0.068	0.758	0.717	0.052	0.798	0.076	0.039	3.585	0.332
Ta	0.012	0.011	0.009	0.014	0.010	0.025	0.012	0.472	0.023
Pb	0.050	1.311	1.357	0.057	5.543	0.056	0.045	0.051	0.037
Th	0.080	4.115	4.020	0.253	5.356	0.028	0.014	0.108	0.012
U	0.018	1.203	1.183	0.052	1.467	0.016	0.009	0.015	0.007
La	0.047	27.60	27.10	0.195	40.63	0.021	0.013	5.399	0.024
Ce	0.044	31.31	30.57	0.218	44.92	0.017	0.013	17.18	0.136
Pr	0.011	2.278	2.110	0.018	3.276	0.008	0.006	3.448	0.034
Nd	0.084	6.235	5.527	0.107	9.175	0.104	0.090	19.53	0.244
Sm	0.062	1.458	1.313	0.071	2.220	0.060	0.058	5.391	0.139
Eu	0.019	0.556	0.558	0.024	0.909	0.018	0.015	1.637	0.046
Gd	0.068	2.378	2.460	0.104	4.124	0.107	0.062	5.575	0.201
Tb	0.009	0.433	0.447	0.014	0.746	0.013	0.007	0.814	0.040
Dy	0.052	3.391	3.220	0.132	5.710	0.059	0.049	5.101	0.343
Ho	0.018	0.729	0.730	0.038	1.277	0.015	0.011	0.967	0.090
Er	0.050	2.250	2.093	0.159	3.794	0.051	0.048	2.542	0.320
Tm	0.013	0.319	0.308	0.028	0.552	0.011	0.010	0.355	0.054
Yb	0.120	2.198	2.080	0.302	3.666	0.075	0.067	2.148	0.446
Lu	0.018	0.308	0.294	0.065	0.545	0.013	0.012	0.312	0.075
Sum LREE	0.25	68.88	66.62	0.61	100.22	0.21	0.18	50.95	0.58
Sum HREE	0.35	12.01	11.63	0.84	20.42	0.35	0.27	17.81	1.57
Sum REE	0.62	81.44	78.80	1.47	121.55	0.58	0.46	70.40	2.19

Analysed phases are primary crystals except those marked as type-2 (cpx-2 of 72688 sample).

amphibole that is higher than those described in peridotite xenoliths, with amphiboles generated in the mantle wedge above subduction zones (supra-subduction amphiboles of Coltorti *et al.* 2007*a*).

Clinopyroxene in lherzolite 65290 from the Cerro Pelado maar displays completely different REE and trace element patterns to the previous lherzolite. It shows a peculiar upwards-convex shape of LREE patterns (with the peak located at Nd) combined with low HREE content (Lu_N down to 9 × Ch). Incompatible element-normalized patterns show a positive fractionation up to the REE where the pattern becomes almost flat, except for a small Ti negative anomaly (Fig. 8). Orthopyroxene (and olivine) does not mimic the REE patterns of coexisting clinopyroxene, instead showing a marked positive fractionation in the REE profiles. Incompatible element patterns are more spiky than those of the coexisting clinopyroxene but fluctuating close to 0.1–1 × Ch values (Fig. 8). A positive Zr–Hf anomaly in the Cerro Pelado orthopyroxene contrasts with the small negative one in El Aprisco.

Similar LREE–Th–U-enriched clinopyroxenes to those of lherzolite 72688 have been described in the Olot lherzolite xenolith suite (Bianchini *et al.* 2007; Galán *et al.* 2008), but the upwards-convex LREE shape has been only described in Olot harzburgites, although displaying a more severe HREE–Zr–Ti depletion (Bianchini *et al.* 2007). Fe-rich lherzolites from the northermost El Palo volcano (Bianchini *et al.* 2010) show clinopyroxene REE patterns similar to those from the Cerro Pelado lherzolite 65290, although with lower total REE content and less prominent convex shape at the MREE. Moreover, clinopyroxene from the Cerro Pelado lherzolite also shows a slightly

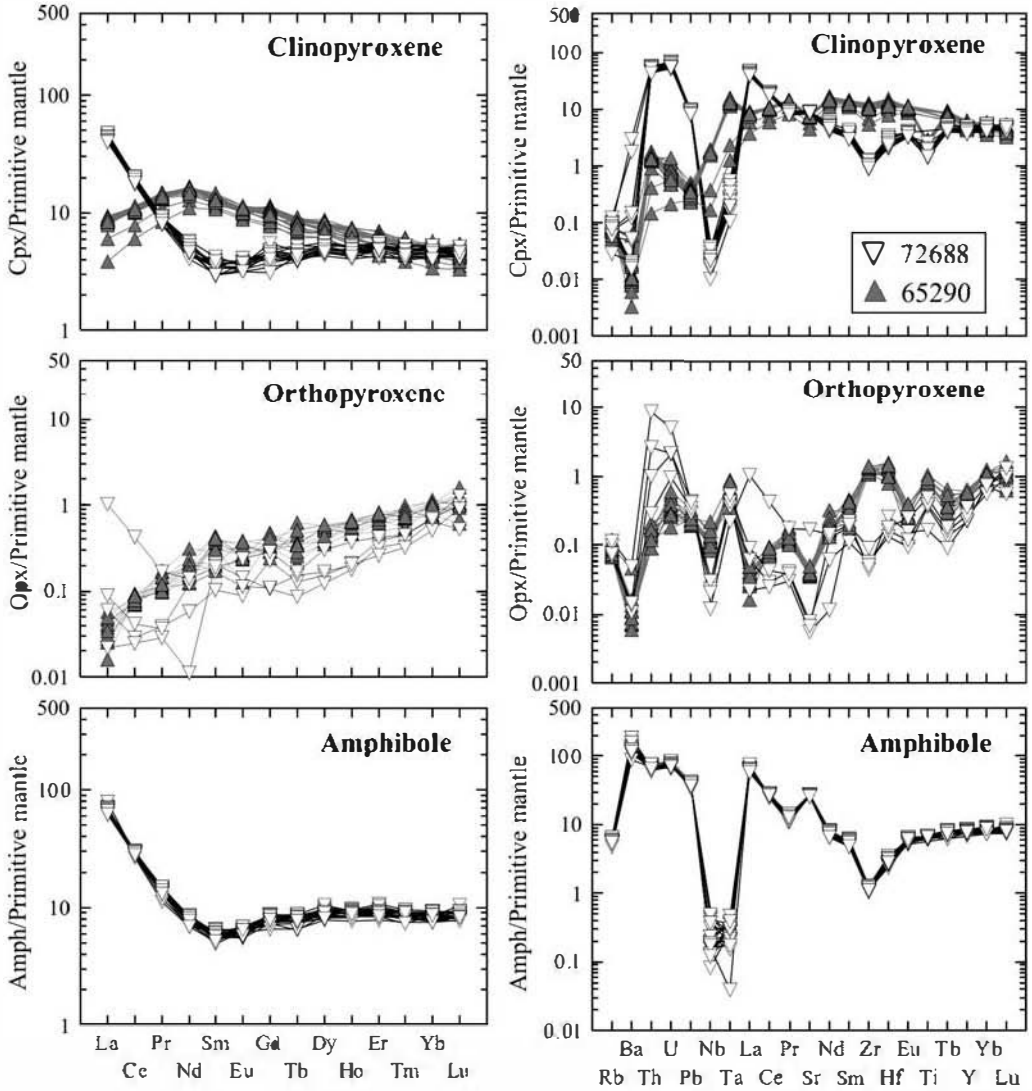

Fig. 8. Primordial mantle-normalized REE and trace element patterns for minerals in the Calatrava peridotite xenoliths. Normalizing values from McDonough & Sun (1995).

higher Zr–Hf–Ta–(Nb)–Y content than those from El Pale. The trace element content of clinopyroxenes from the SE Spain peridotite xenoliths (Beccaluva *et al.* 2004) are completely different to those of Iberian alkaline volcanic fields.

Whole-rock composition

Major and trace elements

Whole-rock major and trace element composition of Calatrava mantle xenoliths are reported in Table 4. They are close to primordial mantle composition or moderately depleted, but their lower Ni, Cr and MgO content when compared to other Spanish mantle xenolith suites (Fig. 9) suggests a more fertile lithospheric mantle composition beneath central Spain. In most samples the Al_2O_3, CaO, FeO and TiO_2 content exibits negative correlations with MgO (Fig. 9), which is a common feature in mantle xenolith suites (e.g. Downes 2001; Ackerman *et al.* 2007; Bianchini *et al.* 2007). This is attributed to depletion during partial melting of the lithospheric mantle (Niu 1997). The most clinopyroxene-rich samples of Calatrava xenoliths (including wehrlite 72674) define a change in the

slope of this compositional trend or an opposite evolution (e.g. positive Al_2O_3 and SiO_2 correlations with MgO) (Fig. 9). The wehrlite sample (72674) shows the most extreme composition of this trend (the highest FeO and TiO_2, and the lowest SiO_2, Al_2O_3 and Cr–Ni, content).

Most of the studied Calatrava lherzolites have high Mg-numbers (0.91–0.92), which are close to primordial mantle estimates (Table 4). However, lower Mg-numbers were determined for wehrlite (0.87, Table 4) and the Ti–Fe-rich lherzolite 65294 (0.89, Table 4). Lower Mg values have been found in other Calatrava lherzolites (see Bianchini *et al.* 2010), which also show a higher Fe-rich character than our studied xenoliths (Fig. 9).

Whole-rock REE patterns are varied in Calatrava xenoliths (Fig. 10). Lherzolites from the El Aprisco centre show a wide compositional trend varying from LREE-enriched steep patterns (72691 sample), through the downwards-convex shape of LREE patterns (72688 sample), identical to those of its corresponding clinopyroxene (see also Fig. 8), towards the slightly negative REE patterns (although slightly upwards-convex in the LREE) (sample 55569) (Fig. 10a). The two samples with lower LREE content are either anhydrous (72690) or contain very minor modal amounts of amphibole (55569). They have similar trace element patterns to the least refractory Olot lherzolites (Beccaluva *et al.* 2004).

Xenoliths from the Cerro Pelado centre show a more homogeneous shape of REE patterns from a LREE-enriched (e.g. wehrlite 72674) to a slightly upwards-convex LREE pattern, similar to its corresponding clinopyroxene (sample 65290) (Fig. 10b). As for the major elements, lherzolites from the El Pale centre (Bianchini *et al.* 2010) show REE patterns more similar to those of the Cerro Pelado lherzolites. Most of the LREE-enriched patterns are attributed to cryptic metasomatism, their variability related both to the nature of the metasomatic agent and the efficiency of the metasomatic process (e.g. Bianchini *et al.* 2007).

In addition to LREE, studied Calatrava xenoliths are also enriched in LILE, Th and U (Fig. 10), although there is some scattering in the data owing to their low trace element concentrations, sometimes below analytical detection limits (Table 4). By contrast, the less LREE-enriched samples show the lowest LILE, P, Th and U content. Most lherzolite xenoliths from the El Aprisco centre display Nb–Ta (Zr–Hf and Ti) negative anomalies in trace element patterns (Fig. 10c).

Sr–Nd isotopes

Isotopic data for the Calatrava lherzolites define two overlapping compositional fields, depending on the sampled volcanic centre. El Aprisco lherzolites have slightly more radiogenic Sr ($^{87}Sr/^{86}Sr$ ratios 0.7035–0.7044) than the Cerro Pelado samples ($^{87}Sr/^{86}Sr$ ratios 0.7032–0.7037) (Table 5) (Fig. 11). Lherzolite xenoliths from this latter volcanic centre show a composition more similar to the host magmas than xenoliths from El Aprisco (Fig. 11). The isotopic field of the Cerro Pelado lherzolites includes the compositional field defined by peridotite xenoliths from the El Pale volcano (Bianchini *et al.* 2010). The whole lherzolite isotopic field defines a wider compositional field than that of their host magmas. This suggests a slightly more enriched character of the Calatrava xenoliths when compared to lithospheric–asthenospheric mantle sources of the host alkaline ultrabasic volcanic magmas. This enriched isotopic signature is remarkable when compared to mantle xenoliths from the other Iberian Cenozoic intraplate alkaline volcanic field (Olot province), which plot towards the depleted mantle composition (Fig. 11) (Bianchini *et al.* 2007). Sr–Nd data from lherzolite xenoliths from the Tallante centre (SE Spain) are highly heterogeneous, plotting along the whole mantle array (not shown) (Beccaluva *et al.* 2004).

Calatrava mantle xenoliths have geochemical affinities to the HIMU-source of ocean island basalts (OIB) and to the EAR, recently called the common mantle reservoir (CMR) of the Circum-Mediterranean anorogenic Cenozoic igneous (CiMACI) province (Lustrino & Wilson 2007). The Sr–Nd isotopic composition of the Calatrava xenoliths shows many similarities with mantle xenoliths from northern domains of the French Massif Central (Downes *et al.* 2003) or those from the Rhön region of Germany (Witt-Eickschen & Kramm 1997).

Discussion

Melting and depletion of the mantle sources of the xenoliths

Clinopyroxene is the main host for HREE in the Calatrava spinel peridotites and, consequently, the degree of partial melting can be estimated by its trace element content (Norman 1998). Although the dataset is limited to two samples, Ti and Na show positive correlation with HREE in clinopyroxene and, thus, the use of Norman's modelling is appropriate. Modelling indicates low degrees of melting for both lherzolite xenoliths, irrespective of the type of melting (batch or fractional), yielding less than 5% of partial melting (Fig. 12). As proposed by several authors (Frey *et al.* 1985; Takazawa *et al.* 2000) for other suites, the major element abundances of the studied Calatrava peridotites could also be used to roughly estimate degrees

Table 4. *Major (wt%) and trace element (ppm) whole-rock analyses of the Calatrava mantle xenoliths*

	El Aprisco						Cerro Pelado				
Sample	55569	55570	72688	72689	72690	72691	58498	65290	65294	65298	72674
SiO_2	43.62	44.72	43.76	44.36	44.04	44.2	44.52	44.51	43.94	44.67	42.35
TiO_2	0.10	0.04	0.12	0.11	0.10	0.06	0.06	0.20	0.43	0.13	0.36
Al_2O_3	2.92	1.86	3.47	4.01	3.73	2.81	2.93	3.76	3.03	3.32	1.84
Fe_2O_3	8.8	8.52	9.11	9.05	9	8.63	8.27	8.75	10.51	8.6	12.99
MnO	0.13	0.13	0.13	0.13	0.13	0.13	0.13	0.13	0.15	0.13	0.16
MgO	41.35	43.46	40.16	40.01	40.05	42.16	41.93	37.89	37.02	41.01	36.92
CaO	2.51	1.29	3.75	2.96	2.49	2.03	2.34	3.28	3.85	3.12	5.25
Na_2O	0.23	0.35	0.28	0.29	0.32	0.49	0.36	0.36	0.32	0.3	0.32
K_2O	bdl	0.13	0.04	0.05	bdl	0.05	0.04	0.07	0.21	0.03	0.1
P_2O_5	0.02	0.07	0.02	0.01	0.01	0.02	0.02	0.03	0.05	0.03	0.07
Total	99.69	100.57	100.85	100.98	99.88	100.58	100.59	98.98	99.51	101.33	100.36
Mg#	0.92	0.92	0.91	0.91	0.91	0.92	0.92	0.91	0.89	0.92	0.87
Ba	16	41	41	23	10	74	38	21	35	10	25
Rb	bdl	bdl	bdl	bdl	bdl	bdl	bdl	bdl	3	bdl	bdl
Sr	5	58	45	14	3	60	49	28	41	26	43
Th	bdl	0.52	0.8	0.6	0.16	1.29	0.45	bdl	0.33	0.15	0.27
U	bdl	0.16	0.29	0.18	0.11	0.22	0.12	bdl	bdl	bdl	bdl
Zr	bdl	bdl	bdl	bdl	6	bdl	bdl	19	15	bdl	14
Nb	bdl	5.2	bdl	bdl	bdl	6.8	bdl	1.4	2.8	1	3.4
Y	2.6	1.5	3.7	2.8	2.7	4.1	2.6	4.1	4	3.4	3.2
Sc	14	10	16	14	12	13	14	16	13	15	15
V	59	22	74	54	50	36	50	68	79	62	73

Co	98	107	101	89	100	107	100	92	110	97	119
Cr	1940	2180	2510	1870	2310	2680	2730	2610	2440	2230	1340
Ni	1730	1990	1730	1570	1710	1900	1790	1520	1790	1680	1000
Ta	bdl	0.13	bdl	bdl	bdl	bdl	bdl	0.13	0.22	bdl	0.17
Hf	bdl	bdl	bdl	bdl	0.2	bdl	bdl	bdl	0.5	bdl	0.5
La	0.21	4.66	5.37	2.03	0.34	5.74	3.31	1.55	3.85	2.07	3.47
Ce	0.4	8.29	7.13	2.59	0.65	11.8	9.09	4.31	7.09	4.03	6.54
Pr	0.06	0.81	0.44	0.17	0.09	1.37	1.16	0.62	0.95	0.45	0.88
Nd	0.4	2.48	1.33	0.78	0.51	5.13	3.7	2.9	4.07	1.74	3.85
Sm	0.17	0.46	0.29	0.22	0.18	1.15	0.74	0.83	1.01	0.42	1.01
Eu	0.07	0.14	0.12	0.10	0.09	0.34	0.23	0.29	0.34	0.15	0.34
Gd	0.3	0.37	0.41	0.3	0.27	0.9	0.52	0.8	0.96	0.44	0.88
Tb	bdl	bdl	bdl	bdl	bdl	0.14	bdl	0.13	0.15	bdl	0.13
Dy	0.39	0.25	0.58	0.44	0.42	0.74	0.42	0.76	0.82	0.52	0.68
Ho	bdl	bdl	0.13	bdl	bdl	0.14	bdl	0.14	0.15	0.11	0.11
Er	0.27	0.14	0.41	0.3	0.3	0.39	0.25	0.4	0.39	0.36	0.29
Tm	bdl	bdl	0.06	bdl	bdl	0.06	bdl	0.06	0.05	0.06	bdl
Yb	0.27	0.13	0.39	0.31	0.33	0.37	0.24	0.39	0.31	0.37	0.2
Lu	0.05	bdl	0.06	0.05	0.05	0.05	0.04	0.06	0.05	0.06	bdl
Ol	67.9	64.5	62.5	55.6	59.8	61.7	62.6	54.4	57.5	60.7	69.3
Cpx	13.8	6.0	16.7	13.2	12.6	9.5	11.4	17.7	22.7	14.9	28.4
Opx	15.8	28.5	17.4	27.5	24.8	26.3	24.7	25.6	17.9	22.9	1.5
Sp	2.5	1.0	3.4	3.7	2.9	2.6	1.3	2.3	2.0	1.5	0.1
F*	13.1	20.9	8	7.9	8.3	17.3	16.8	1.5	–	13.3	–

*Partial melting degrees estimated using Takazawa *et al.* (2000) method.

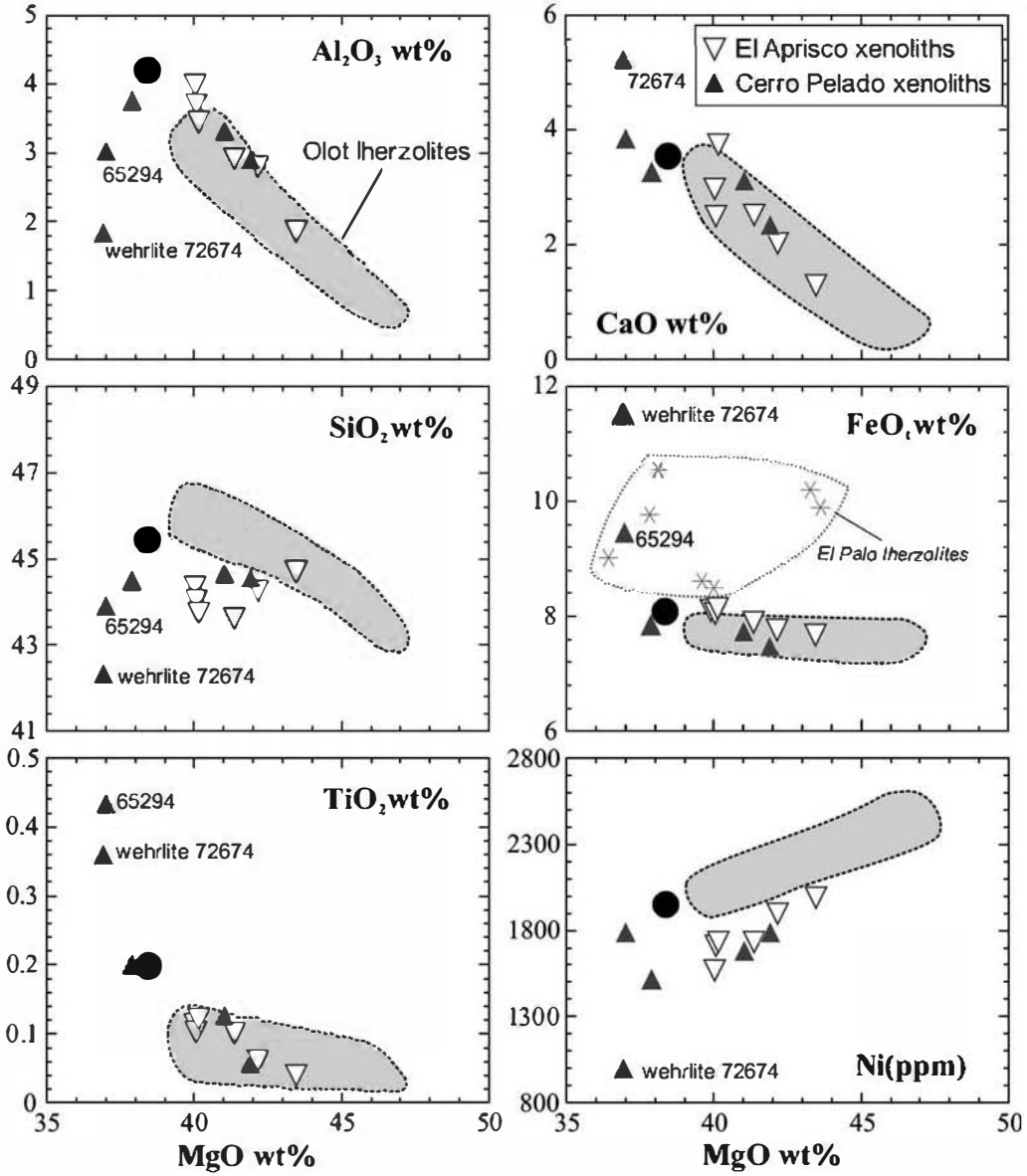

Fig. 9. Variations in whole-rock major oxides with MgO (wt%). Data of lherzolite xenoliths from NE Spain (Olot) (grey field) (Bianchini *et al.* 2007; Galán *et al.* 2008: excepting sample BB.12.030) are shown for comparison. The data for Tallante xenoliths overlap the Olot field (see also Bianchini *et al.* 2007). Data from peridotite xenoliths from the other Calatrava centre (El Palo: Bianchini *et al.* 2010) is only included in the MgO v. FeO_t plot, as they mostly overlap with our data in other diagrams. The composition of primitive mantle (McDonough & Sun 1995) is represented by a filled circle.

of melting of a compositionally homogeneous source in a melting residue model. Using batch melting modelling with a $K_d^{olivine}{}_{Fe^{2+}/Mg}$ of 0.3 and assuming the primitive mantle values of McDonough & Sun (1995) as source composition, we find that the series of peridotites reflect residues from approximately 2 to 21% melting (lherzolites 65290 and 55570, respectively; Table 4). Inferred degrees of melting for lherzolites 72688 and 65290 estimated using both methods, whole-rock major element composition and clinopyroxene trace element content, yield similar results (although

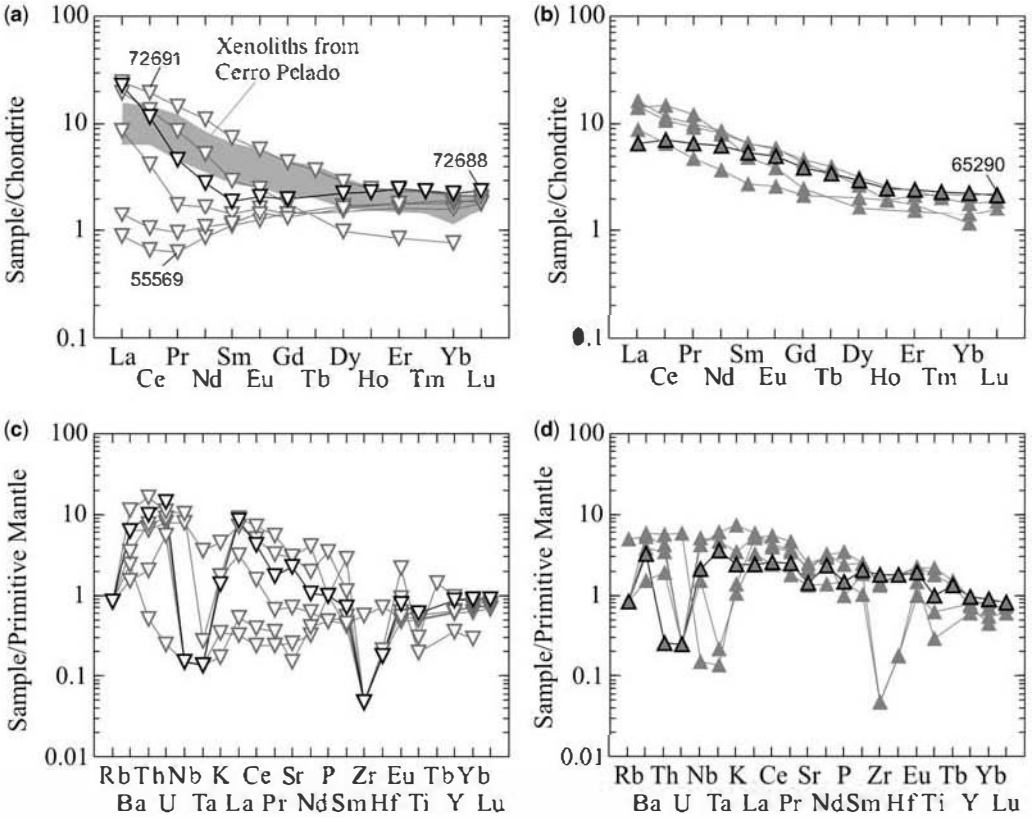

Fig. 10. Chondrite-normalized REE patterns and primordial mantle-normalized trace element patterns for whole rocks of the Calatrava peridotite xenoliths. (a), (c) REE and trace element patterns of lherzolite xenoliths from the El Aprisco centre. (b), (d) REE and trace element patterns of mantle xenoliths from the Cerro Pelado centre. Normalizing values from McDonough & Sun (1995).

Table 5. *Whole-rock (Sr–Nd) isotopic composition of the Calatrava mantle xenoliths*

	$^{87}Sr/^{86}Sr$	εSr	$^{143}Nd/^{144}Nd$	εNd
El Aprisco				
55569	0.704350 ± 06	−2.1	0.512976 ± 63	6.6
55570	0.703515 ± 06	−14.0	0.512847 ± 16	4.1
72688	0.703686 ± 05	−11.6	0.513073 ± 22	8.5
72689	0.703768 ± 06	−10.4	0.513051 ± 43	8.1
72690	0.704251 ± 05	−3.5		
72691	0.703675 ± 05	−11.7	0.512804 ± 03	3.2
Cerro Pelado				
58498	0.703675 ± 06	−11.7	0.512777 ± 03	2.7
65290	0.703200 ± 06	−18.5	0.512957 ± 17	6.2
65294	0.703198 ± 06	−18.5	0.512950 ± 06	6.1
65298	0.703331 ± 05	−16.6	0.512922 ± 05	5.5
72674	0.703219 ± 05	−18.2	0.512917 ± 05	5.4

Uncertainties for the $^{87}Sr/^{86}Sr$ and $^{143}Nd/^{144}Nd$ ratios are 2σ (mean) errors in the last two digits.

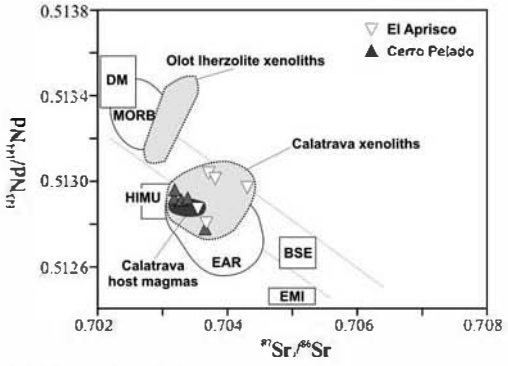

Fig. 11. $^{143}Nd/^{144}Nd$ v. $^{87}Sr/^{86}Sr$ diagram for the Calatrava mantle xenoliths compared to the composition of the host volcanic magmas (López-Rniz *et al.* 2002). The compositional field of NE Spain (Olot) lherzolite xenoliths (Bianchini *et al.* 2007) is also reported. Mantle end members (DM, MORB, HIMU, BSE and EMI) are from Zindler & Hart (1986). EAR after Downes *et al.* (2003).

the whole-rock method gives higher F values). The samples wehrlite 72674 and lherzolite 65294 have not been used in this model as they have a more fertile composition than primitive mantle estimates. Nevertheless, there is no evidence for such a high partial melting degree in the Calatrava xenoliths. The absence of harzburgites in the studied xenoliths contrasts with the common presence of this rock type in other mantle xenolith suites that have suffered degrees of melting higher than 10% (e.g. Olot mantle xenoliths: Galán *et al.* 2008). These F values are also higher than those estimated by the major element chemistry of minerals

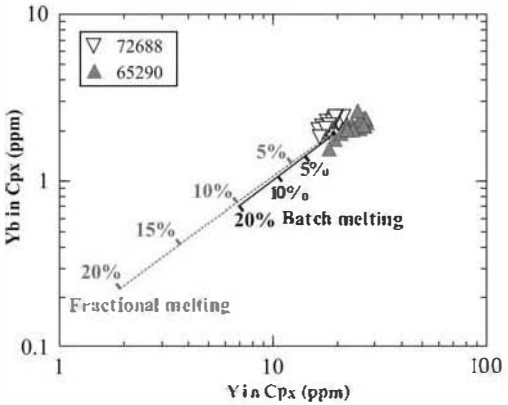

Fig. 12. Partial melting results for Y and Yb in clinopyroxene, following the model of Norman (1998). Both fractional and batch melting suggest low degrees of melting (< 5%) for the analysed lherzolites. See the text for further explanation.

(specially the low Cr-numbers of primary spinel; see Fig. 6), suggesting that with the current dataset most of the Calatrava peridotite xenoliths are slightly–moderately depleted and their chemistry is close to fertile mantle composition.

The moderate degree of melting of the Calatrava peridotites contrast with data from the others Iberian mantle xenolith suites. The Olot lherzolites yield modelled melting fractions up to 17% (Bianchini *et al.* 2007), being markedly higher when involving harzburgite types (up to 30–40% of melting: Bianchini *et al.* 2007; Galán *et al.* 2008). In SE Spain, the presence of harzburgite and opx-rich lherzolite xenoliths also suggests a large degree of partial melting of lithospheric mantle (Beccaluva *et al.* 2004; Shimizu *et al.* 2004), although detailed partial melting models have not been applied. The high Cr-numbers of spinel from peridotite xenoliths from SE Spain volcanics is also in accordance with a wider and higher degree of partial melting, and a more residual nature of those mantle xenoliths (Fig. 6). The lower Cr, Ni and MgO content of the Calatrava xenoliths (Table 4 and Fig. 9) is in agreement with a more fertile character of the lithospheric mantle beneath central Spain.

A discussion on the possibility that the xenoliths may have a similar composition to the sources for the alkaline Calatrava volcanic field is beyond the scope of this paper. We note, however, that the relatively fertile character of most xenoliths and the Sr–Nd isotopic signatures of them suggest a genetical relationship with the associated volcanism. Cebriá & López-Ruiz (1995) suggested that the Calatrava volcanic rocks constitute a suite generated by variable degrees of partial melting (F = 5–17%) of a phlogopite (amphibole)-bearing enriched mantle source with 1.2–10 times the primitive mantle values for incompatible elements. Most of the studied peridotite xenoliths show this compositional range, especially the phlogopite-bearing xenoliths from the Cerro Pelado centre (Fig. 10). Nevertheless, the HREE depleted character of most of the Calatrava volcanic rocks is indicative of garnet-bearing sources (Cebriá & López-Ruiz 1995; López-Ruiz *et al.* 2002) and, therefore, they may have a deeper mantle derivation.

Origin of the glasses

The presence of glass veins in mantle xenoliths may be the result of several different formation mechanisms: (1) decompression melting during transport; (2) host magma infiltration; (3) reaction between a percolating melt and host peridotite at mantle depths; and (4) involvement of previously formed metasomatic phases (e.g. amphibole, phlogopite) during partial melting in the mantle (Yaxley *et al.*

1997; Yaxley & Kamenetsky 1999; Coltorti *et al.* 2000). The contrasting geochemical composition of analysed interstitial glasses in the Calatrava xenoliths with ultrabasic host nephelinite–melilitite magmas (Fig. 7) suggests that host magma infiltration could not explain the origin of these low melt fractions.

Most of the glasses in the Calatrava xenoliths contain microcrysts of clinopyroxene, olivine and spinel (Fig. 3e–h). The Al^{VI}/Al^{IV} ratios close to 1 in this newly formed clinopyroxene (cpx-2, Table 1) indicate high-pressure crystallization (Aoki & Kushiro 1968). As discussed above, the chemistry of cpx-2 related to glasses leads to similar geobarometric estimates as for primary clinopyroxene (Table 2). Thus, the formation of glasses might have occurred at mantle depths, and these metasomatically enriched mantle fragments were later accidentally entrained as xenoliths in the Calatrava alkaline magmas. The vesicular aspect of the intergranular glasses and veins (Fig. 3e–h), typical of volcanic–subvolcanic emplacement levels, suggests that volatile exsolution after xenolith entrainment has occurred.

The variability observed in glass composition between different Calatrava peridotite xenoliths implies variations in the metasomatic agent and in the peridotite minerals involved in partial melting processes. Glasses from the Cerro Pelado xenoliths show a great similarity in chemical composition with experimental studies on the low of degree melting of peridotites, which usually yield trachyandesitic glass compositions (Draper & Green 1997; Perinelli *et al.* 2008*a*). The glass composition is used as a good geochemical indicator of the metasomatic agent (Coltorti *et al.* 2000). The major element composition of glasses from the Cerro Pelado xenoliths are indicative of a Na-alkali silicate metasomatism owing to its high $TiO_2 + K_2O$ content (in the range of 5.3–7.2) (Table 1). Moreover, the involvement of an alkaline metasomatism in the Cerro Pelado xenoliths is also consistent with the trace element geochemistry of their primary clinopyroxenes, as discussed later. The melts were partially modified by crystallization of a secondary assemblage of clinopyroxene + olivine + spinel or by reaction with primary peridotite minerals. The origin of cellular or sieve textures in peridotite minerals (e.g. spinel, Fig. 3f) is consistent with incongruent dissolution, in which the part of the crystal in direct contact with an interstitial melt is first dissolved, followed by nucleation and growth of the new phase. Strong contrasts in Ti and Cr content between primary spinel and the new cellular spinel-2 is consistent with the presence of melt (Shaw & Dingwell 2008). However, the involvement of previous metasomatic hydrous phases in the melting reaction is not precluded, as suggested in other cases (Yaxley *et al.* 1997; Yaxley & Kamenetsky 1999), but this deserves better constrained mineral data in more detailed studies. Glass in wehrlite 72674 forms some veining, indicating melt mobility through grain boundaries of the peridotite matrix. However, an interaction of peridotite with its host melt has not been observed.

Interstitial glass in lherzolite 72689 from El Aprisco is markedly subalkaline (Fig. 7). Its chemical composition, characterized by extremely low K (and Ti) content (Table 1), is similar to glasses originated during carbonatitic metasomatism (Coltorti *et al.* 2000) or by infiltration of subduction-related carbonate–silicate melts (Demény *et al.* 2004). Nevertheless, the Qtz–Hy-normative composition of this glass, combined with its slightly peraluminous character (Table 1), precludes a carbonate-rich percolant agent. SiO_2-oversaturated glasses with low Ti–P–K content in peridotite xenoliths are usually interpreted as having originated by amphibole breakdown (Chazot *et al.* 1996; Ban *et al.* 2005) or by infiltration of subduction-derived silicate melts–aqueous fluids (Ishimaru & Arai 2009) or by a combination of both processes. Glass in hydrous lherzolite 72689 appears in a complex reaction zone involving the primary lherzolite minerals and producing a second crystal generation of clinopyroxene, olivine and spinel (Fig. 3e). These low-K glasses are uncommon in Iberian mantle xenoliths but they are described in some other xenolith suites (Chazot *et al.* 1996; Ismail *et al.* 2008). Locally, the melting has involved the former amphibole present in spinel aureoles. This is supported by the similar Na_2O/K_2O ratios displayed by amphibole and glass composition in lherzolite xenoliths from El Aprisco (glasses: $Na_2O/K_2O = 80–180$; amphiboles: $Na_2O/K_2O = 45–700$), and the tendency for the subalkaline composition of glasses generated in partially melted natural amphibole-bearing ultramafic rocks (Perinelli *et al.* 2008*a*). Moreover, the composition of the interstitial glass in lherzolite 72689 is very similar to that of amphibole-derived melts from lherzolites from West Eifel (Ban *et al.* 2005), including typical low abundances of P_2O_5 and TiO_2, although El Aprisco glasses have a lower K_2O content, in accordance with the extremely low-K character of the amphibole in this sample. The absence of phlogopite in the El Aprisco xenoliths would also explain the low Ti and K content of analysed interstitial glasses of lherzolite 72689.

Metasomatism of the xenoliths

Evidence of metasomatism in the Calatrava peridotites is provided by: (i) a strong enrichment in LREE, Th and U in clinopyroxene; (ii) the

occurrence of metasomatic hydrous minerals (amphibole, phlogopite); and (iii) the presence of intergranular glasses. Most of the studied xenoliths display evidence of modal metasomatism, with the development of reaction zones and aureoles at the expense of spinel (except for the lherzolite sample 72690 from El Aprisco). The involvement of a previous silicate metasomatism is supported by the trace element chemistry of primary clinopyroxenes, as discussed further below.

The presence of LREE-rich clinopyroxenes with negative anomalies in Nb, Ta and Zr (but no Hf) has been also described in some spinel lherzolites from Olot (sample Olt8: Bianchini *et al.* 2007), the French Massif Central (Downes *et al.* 2003; Touron *et al.* 2008) and Eifel (Witt-Eickschen & Kramm 1997) within the CiMACI province. Some of these xenoliths lack volatile-rich phases, so the clinopyroxene composition is a primary mantle feature related to the infiltration of LREE–Th–U-enriched silicate melts (some of them of probable subalkaline affinity: Touron *et al.* 2008). Clinopyroxenes from Calatrava mantle xenoliths have a high Ti/Eu and moderate $(La/Yb)_N$ (Fig. 13), as well as low $(Nd/Hf)_N$ (<2.3) and $(Gd/Ti)_N$ (<4.8), which are geochemical indicators that the metasomatic medium was essentially a silicate melt rather than a carbonate-rich melt fraction (Coltorti *et al.* 1999; Xu *et al.* 2003; Ismail *et al.* 2008).

In terms of REE (and HFSE) content, the metasomatic amphibole perfectly mimics the coexisting clinopyroxene (sample 72688) and shows LREE enrichment at a comparable HREE content (10 × Ch). The same trace element mimicry is also displayed by the small neoformed type-2 clinopyroxene which shows similar REE patterns

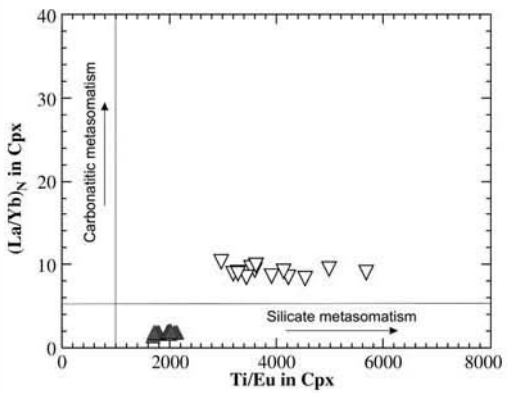

Fig. 13. $(La/Yb)_N$ v. Ti/Eu in clinopyroxenes from Calatrava lherzolite xenoliths. (La/Yb) ratios are normalized to chondrite values from McDonough & Sun (1995).

to the primary crystals. Trace element content might be controlled by intermineral distribution coefficients more than by extrinsic parameters (P, T, fO_2), and K_d^{REE} for clinopyroxenes–amphiboles is fairly close to 1 (e.g. Bianchini *et al.* 2007; Galán *et al.* 2008). Geochemical features of amphiboles from mantle xenoliths are good indicators of the metasomatic agents involved. The low Ti–Nb–Zr content of amphiboles from the Calatrava xenoliths (and their correlative high Zr/Nb and Ti/Nb ratios, >25 and >50 000, respectively) are chemical features indicative of suprasubduction amphiboles (S-Amph types of Coltorti *et al.* 2007*a*), and they might record subduction-related metasomatic components, even in a multistage metasomatic history. Glass chemistry in hydrous lherzolite 72689 from El Aprisco also suggests the involvement of a subduction-related metasomatism (see the previous subsection).

The estimated composition of melts in equilibrium with clinopyroxene and amphibole from lherzolite 72688 points to the involvement of a metasomatic agent with marked Nb–Ta negative anomalies and flat HREE patterns, very different to the incompatible trace element patterns shown by the host ultrabasic alkaline melts (Fig. 14). The Nb–Ta trough (and prominent Th–U–Pb positive anomalies) in all of the primary minerals of the studied Calatrava mantle xenolith 72688 (clinopyroxene, orthopyroxene and olivine) suggests that an important metasomatic event occurred before xenolith entrapment within the lithospheric mantle. Other Calatrava mantle xenoliths also show Nb–Ta negative (and Th–U positive) anomalies in whole-rock composition (mainly from the El Aprisco centre), which suggests that this kind of metasomatism was common in the lithospheric mantle of central Spain. Most geochemical agents with prominent Th–U positive and Nb–Ta negative anomalies are related to continental lithosphere, suggesting that this chemical imprint could be inherited from some kind of subduction-derived metasomatism. Contamination by Variscan continental crust in mantle sources has recently been proposed, by Prelevic *et al.* (2008), as the origin for the nearby Cenozoic lamproites from SE Spain. However, no significant contamination by continental crust in the Calatrava peridotites is recorded by the isotopic data.

We have also estimated the composition of melts in equilibrium with clinopyroxene from lherzolite 65290 (from the Cerro Pelado centre) (Fig. 14a). The trace element content of the inferred melts are comparable to the undersaturated magma found in the area, suggesting a strong link between metasomatism and the magmatism of the Calatrava volcanic field in this case. This is in agreement with the less radiogenic Sr isotope composition of this

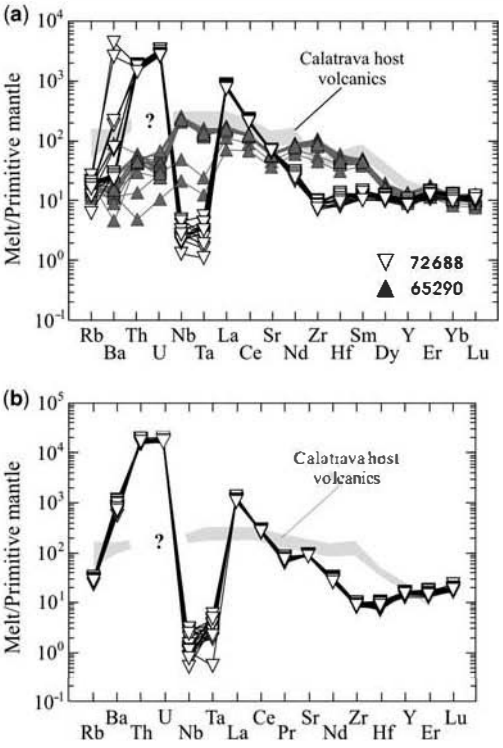

Fig. 14. Trace element composition of melts in equilibrium with (a) clinopyroxenes and (b) amphiboles from Calatrava lherzolites. (a) Data calculated using cpx–basaltic melt partition coefficients (Hart & Dunn 1993), except for Rb (Foley *et al.* 1996) and Ta (Adam & Green 2003). (b) Data calculated using amph–melt partition coefficients of La Tourrette *et al.* (1995). The average composition of Calatrava host volcanics is from Cebriá & López-Ruiz (1995). Normalizing values for primitive mantle from McDonough & Sun (1995).

xenolith compared to those from El Aprisco, and the coincidence in isotopic composition with the host basaltic magmas (Table 5 and Fig. 11). It is also in agreement with the composition of associated interstitial glasses, which involves a Na-rich alkaline melt. Thus, different silicate metasomatic agents are involved in the genesis of the wide range of Calatrava peridotite xenoliths.

Cenozoic Calatrava volcanics record a HIMU component in their lithospheric–asthenospheric mantle sources based on their Sr–Nd–Pb isotopic composition (López-Ruiz *et al.* 2002). The Sr–Nd isotopic composition of mantle xenoliths from central Spain also plot close to the HIMU compositional field (Fig. 11). Nevertheless, studied mantle xenoliths reflect a previous subduction-related metasomatic imprint. Isotopic composition of mantle xenoliths from central Spain could be the result of the mixing between a more depleted mantle source (asthenospheric component) and a deeply recycled enriched component, as recently suggested in some French Massif Central mantle xenoliths (Touron *et al.* 2008), making arguable the involvement of a HIMU component. In this sense, mantle xenoliths from the northernmost El Pale volcano indicate a long-term recycling of oceanic subducted components (Bianchini *et al.* 2010) that is not recorded in our studied lherzolite xenolith suite. Thus, additional sampling and new isotope data (Pb, O, etc.) are required to solve this problem.

On the origin of Calatrava wehrlite xenoliths

The presence of ultramafic rock types, which are not likely to be partial melting residues from fertile mantle in peridotite xenolith suites, poses the problem of their origin and significance. Wehrlites are common in many lherzolite and harzburgite xenoliths suites. Their origin has been discussed in terms of cumulates from mafic melts trapped in mantle depths or by reaction of residual wall-rock peridotites with migrating magmatic liquids, either carbonate-rich or subsaturated Fe–Ti-rich silicate melts (e.g. Hauri *et al.* 1993; Coltorti *et al.* 1999; Ionov *et al.* 2005; Beard *et al.* 2007). Wehrlite 75674, from the Calatrava xenoliths, has no cumulate textures, contains some olivine grains showing strain and deformation twins, and the majority of crystals have smooth curvilinear boundaries. Moreover, this wehrlite shows similar geochemical signatures to those of lherzolite 65294 and the other Cerro Pelado xenoliths (Figs 9–11). Thus, our petrographical observations and whole-rock composition rule out a cumulate origin for the Calatrava wehrlite studied.

The similar Al content in the orthopyroxenes from the lherzolites and wehrlites (Fig. 4a) suggest that the original rock was lherzolitic. Moreover, major element trends shown by the Cerro Pelado xenoliths are similar to those described for the Fe-rich lherzolite–wehrlite (LW) series formed by reactive melt percolation in associated lherzolites (Ionov *et al.* 2005). The overlapping of trace element patterns (wehrlite and Cerro Pelado lherzolites have almost identical REE patterns, Fig. 10b) also indicates that wehrlite might have been originated by the transformation of associated slightly residual lherzolites, by percolation of metasomatic melts. Accordingly, associated lherzolites must be the protolith of the wehrlite. The lack of a marked LREE enrichment, in addition to a strong Ti–Fe enrichment of the wehrlite, suggest that the metasomatic agent was not a carbonate-rich silicate melt (Hauri *et al.* 1993; Coltorti *et al.* 1999). This is also in agreement with the lack of carbonatite metasomatism in the Calatrava peridotites, together

with the absence of carbonate-rich magmatism in central Spain.

We suggest that a metasomatic agent had reacted with the primary lherzolite orthopyroxene to produce clinopyroxene and to displace its modal composition towards wehrlite. If this is correct, then the melt must have been undersaturated in silica and relatively rich in Ca, K, Fe and Ti, which would have increased these components in the wehrlite (Fig. 9). In this respect, if we use the whole-rock Mg# and Cpx/Opx modelling of Ionov *et al.* (2005) our Calatrava samples 75674 and 65294 match a model involving a reaction of host peridotites with evolved silica-undersaturated silicate melts (Mg numbers = 0.6–0.7) at low melt/rock ratios (*c.* 2 for *R* parameter = 0.2) (fig. 14 of Ionov *et al.* 2005).

Addressing possible origins for such percolating alkaline silicate melts is complicated. The mineral composition of olivine, clinopyroxene and the scarce spinel of the studied wehrlite xenolith are similar to those obtained in experimental work on metasomatism induced by alkaline magmas of nephelinite composition with upper-mantle peridotites (Perinelli *et al.* 2008*a*). Calatrava volcanism involved silica-undersaturated alkaline melts of either potassic or sodic composition (e.g. Ancochea 1982; López-Ruiz *et al.* 2002), and ultrapotassic magmatism occurred prior to these more sodic alkaline events that carried the studied mantle xenoliths. The similarity in Sr–Nd isotopic ratios of the wehrlite and its host volcanic rocks suggests that the Calatrava alkaline magmatism could have been involved in the genesis of the wehrlites. Furthemore, as explained above, a similar alkaline metasomatic imprint has been described for the associated lherzolite xenoliths.

Conclusions

The mineral chemistry and whole-rock composition of the Calatrava lherzolite xenoliths is typical of peridotites that have undergone small–moderate degrees of partial melting, mostly less than 10%, although the more varied xenolith population described in the literature suggests a more heterogeneous nature for this lithospheric section. Superimposed on this moderately fertile character there is a complex metasomatism of uncertain timing produced by silicate melts. One metasomatic agent (the El Aprisco lherzolite suite) could be genetically associated with subduction-derived components. Another metasomatic agent recorded in the studied peridotite xenoliths (the Cerro Pelado lherzolite suite) is an alkaline silicate melt producing a geochemical signature similar to that of the undersaturated alkaline Calatrava magmatism. Metasomatism related to tholeiitic melts or subducted oceanic crust, as sugested for the Calatrava El Palo lherzolite suite (Bianchini *et al.* 2010), is not recorded in the studied peridotites. This reveals the wide range in upper-mantle heterogeneous composition that can be found beneath a small volcanic province.

The presence of wehrlite types within the studied Calatrava peridotite xenoliths is interpreted as a reaction of host lherzolites with silica-undersaturated silicate melts. The lack of petrographical evidence, the overlapping of trace element content and the Sr–Nd isotopic ratios of wehrlite and associated lherzolites rule out a cumulate origin. The strong Fe–Ti enrichment of the wehrlite indicates that the metasomatic agent was not a carbonate-rich silicate melt. The development of wehrlite types by the reactive percolation of alkaline magmas similar to those that generate the Calatrava volcanic field, but at higher melt/rock ratios than associated lherzolites, must be studied in more detail in future work. Indeed, the possibility of the existence of Fe-rich lherzolite–wehrlite series rocks in the underlying Calatrava upper mantle is insinuated by the present data (see also Bianchini *et al.* 2010).

Most of the metasomatically newly formed minerals mimic the trace element content of the primary phases and, thus, the main metasomatism recorded by studied peridotite xenoliths is likely to be related to 'primary' metasomatism at mantle sources rather than during magma transport.

The proposed sequence of events for the studied Calatrava mantle xenoliths could be as follows.

(1) Cryptic and modal (e.g. amphibole with suprachondritic Ti/Nb and Zr/Nb ratios) metasomatism by subduction-related components. The timing of this metasomatism is unconstrained, although a Tertiary subduction, as suggested in other Cenozoic volcanic fields (Piromallo *et al.* 2008; Bianchini *et al.* 2010), could not be discounted with the current available data.

(2) Localized alkaline metasomatism shortly before magma entrainment as evidenced by some lherzolite xenoliths from Cerro Pelado (sample 65290). This could evolve to widespread replacement towards wehrlite types (sample 72674) at higher rates of melt percolation. This silica-undersaturated silicate metasomatic agent could be associated with early stages of the Cenozoic alkaline magmatism in central Spain.

(3) Partial melting occurred in some xenoliths at mantle depths and related to similar metasomatic agents that have enriched the xenoliths previously. The participation in the melting of the previously metasomatically introduced

phases (e.g. amphibole, phlogopite) is not precluded with the current data.

(4) Erosion of previously metasomatized lithospheric mantle at spinel-facies conditions, at around 35–50 km depth. Rapid decompression would promote the vesiculation and quenching of previously formed interstitial glass, together with localized intergranular recrystallization around spinel and the other peridotite minerals.

Finally, the Sr–Nd isotopic composition of the Calatrava mantle xenoliths plot within the EAR or CMR upwelling mantle beneath Europe; these values represent more enriched signatures than those found in the other Spanish Cenozoic alkaline province (Olot) but show many similarities with mantle xenoliths from the northern domains of the French Massif Central and those from the Rhön region in Germany.

We thank A. F. Larios and J. G. del Tánago for their assistance with the electron microprobe analyses in the CAI of Microscopía Electrónica (UCM). Also J. M. Fuenlabrada Pérez and J. A. Hernández Jiménez from the CAI of Geocronología y Geoquímica (UCM) for their help in analysing samples by TIMS. H. Downes is greatly thanked for her careful English revision and for inviting us to collaborate in this monographic volume. Detailed revision by V. Cvetkovic, T. Ntaflos and M. Coltorti greatly improved the quality of the manuscript. This work was supported by grants CGL-2006-03414 and CGL-2008-05952 of the Ministerio de Educación y Ciencia of Spain. This research also received support from the SYNTHESYS project GB-TAF-2768 funded by the European Community Research Infrastructure Action under the FP6 'Structuring the European Research Area' Programme.

References

Ackerman, L., Mahlen, N., Jelínek, E., Medaris, G. Jr, Ulrych, J., Strnad, L. & Mihaljevic, M. 2007. Geochemistry and evolution of subcontinental lithospheric mantle in Central Europe: evidence from peridotite xenoliths of the Kozákov volcano, Czech Republic. *Journal of Petrology*, **48**, 2235–2260.

Adam, J. & Green, T. H. 2003. The influence of pressure, mineral composition and water on trace element partitioning between clinopyroxene, amphibole and basanitic melts. *European Journal of Mineralogy*, **15**, 831–841.

Albarède, F. 1995. *Introduction to Geochemical Modelling*. Cambridge University Press, Cambridge.

Ancochea, E. 1982. *Evolución espacial y temporal del volcanismo reciente de España Central*. PhD thesis, Complutense University, Madrid.

Ancochea, E. 2004. La región volcánica del Campo de Calatrava. *In*: Vera, J. A. (ed.) *Geología de España*. SGE-IGME, Madrid, 676–677.

Ancochea, E. & Nixon, P. H. 1987. Xenoliths in the Iberian peninsula. *In*: Nixon, P. H. (ed.) *Mantle Xenoliths*. Wiley, Chichester, 119–124.

Aoki, K. & Kushiro, I. 1968. Some clinopyroxenes from ultramafic inclusions in Dreiser Eiher, Eifel. *Contributions to Mineralogy and Petrology*, **18**, 326–337.

Arai, S. 1992. Chemistry of chromian spinel in volcanic rocks as a potential guide to magma chemistry. *Mineralogical Magazine*, **56**, 173–184.

Arai, S. 1994. Characterization of spinel peridotites by olivine–spinel compositional relationships: review and interpretation. *Chemical Geology*, **113**, 191–204.

Ban, M., Witt-Eickschen, G., Klein, M. & Seck, H. A. 2005. The origin of glasses in hydrous mantle xenoliths from the West Eifel, germany: incongruent break down of amphibole. *Contributions to Mineralogy and Petrology*, **148**, 511–523.

Beard, A. D., Downes, H., Mason, P. R. D. & Vetri, V. R. 2007. Depletion and enrichment processes in the lithospheric mantle beneath the Kola Peninsula (Russia): evidence from spinel lherzolite and wehrlite xenoliths. *Lithos*, **94**, 1–24.

Beccaluva, L., Bianchini, G., Bonadiman, C., Siena, F. & Vaccaro, C. 2004. Coexisting anorogenic and subduction-related metasomatism in mantle xenoliths from the Betic Cordillera (southern Spain). *Lithos*, **75**, 67–87.

Bertrand, P. & Mercier, J. C. 1985. The mutual solubility of coexisting ortho- and clinopyroxene: toward an absolute geothermometer for the natural system. *Earth and Planetary Science Letters*, **76**, 109–122.

Bianchini, G., Beccaluva, L., Bonadiman, C., Nowell, G., Pearson, G., Siena, F. & Wilson, M. 2007. Evidence of diverse depletion and metasomatic events in harzburgite–lherzolite mantle xenoliths from the Iberian plate (Olot, NE Spain): implications for lithosphere accretionary processes. *Lithos*, **94**, 25–45.

Bianchini, G., Beccaluva, L., Bonadiman, C., Nowell, G. M., Pearson, D. G., Siena, F. & Wilson, M. 2010. Mantle metasomatism by melts of HIMU piclogite components: new insights from Fe-lherzolite xenoliths (Calatrava Volcanic District, central Spain). *In*: Coltorti, M., Downes, H., Grégoire, M. & O'Reilly, S. (eds) *Petrological Evolution of the European Lithospheric Mantle*. Geological Society, London, Special Publications, **337**, 107–124.

Bonatti, E. & Michael, P. J. 1989. Mantle peridotites from continental rifts to ocean basins to subduction zones. *Earth Planetary Science Letters*, **91**, 297–311.

Brey, G. P. & Köhler, T. 1990. Geothermobarometry in four-phase lherzolites; II, New thermobarometers, and practical assessment of existing thermobarometers. *Journal of Petrology*, **31**, 1353–1378.

Cebriá, J. M. & López-Ruiz, J. 1995. Alkali basalts and leucitites in an extensional intracontinental plate setting: the late Cenozoic Calatrava Volcanic Province (central Spain). *Lithos*, **35**, 27–46.

Chazot, G., Menzies, M. & Harte, B. 1996. Silicate glasses in spinellherzolitefrom Yemen: origin and chemical composition. *Chemical Geology*, **134**, 159–179.

Coltorti, M., Beccaluva, L., Bonadiman, C., Faccini, B., Ntaflos, T. & Siena, F. 2004. Amphibole genesis via metasomatic reaction with clinopyroxene in mantle xenoliths from Victoria Land, Antarctica. *Lithos*, **75**, 115–139.

Coltorti, M., Beccaluva, L., Bonadiman, C., Salvini, L. & Siena, F. 2000. Glasses in mantle xenoliths as

geochemical indicators of metasomatic agents. *Earth Planetary Science Letters*, **183**, 303–320.

COLTORTI, M., BONADIMAN, C., FACCINI, B., GRÉGOIRE, M., O'REILLY, S. Y. & POWELL, W. 2007*a*. Amphiboles from suprasubduction and intraplate lithosperic mantle. *Lithos*, **99**, 68–74.

COLTORTI, M., BONADIMAN, C., FACCINI, B., NTAFLOS, T. & SIENA, F. 2007*b*. Slab melt and intraplate metasomatism in Kapfenstein mantle xenoliths (Styrian Basin, Austria). *Lithos*, **94**, 66–89.

COLTORTI, M., BONADIMAN, C., HINTON, R. W., SIENA, F. & UPTON, B. G. J. 1999. Carbonatite metasomatism of the oceanic upper mantle: evidence from clinopyroxenes and glasses in ultramafic xenoliths of Grande Comore, Indian Ocean. *Journal of Petrology*, **40**, 133–165.

DEMÉNY, A., VENNEMANN, T. W. *ET AL.* 2004. Trace element and C–O–Sr–Nd isotope evidence for subduction-related carbonate–silicate melts in mantle xenoliths (Pannonian Basin, Hungary). *Lithos*, **75**, 89–113.

DOWNES, H. 2001. Formation and modification of the shallow sub-continental lithospheric mantle: a review of geochemical evidence from ultramafic xenolith suites and tectonically emplaced ultramafic massifs of western and central Europe. *Journal of Petrology*, **42**, 233–250.

DOWNES, H., REICHOW, M. K., MASON, P. R. D., BEARD, A. D. & THIRLWALL, M. F. 2003. Mantle domains in the lithosphere beneath the French Massif Central: trace element and isotopic evidence from mantle clinopyroxenes. *Chemical Geology*, **200**, 71–87.

DRAPER, D. S. & GREEN, T. H. 1997. *P–T* phase realtions of silicic, alkaline, aluminous mantle-xenoliths glasses under anhydrous and C–O–H fluid saturated conditions. *Journal of Petrology*, **38**, 1187–1224.

FERNÀNDEZ, M., MARZÁN, I., CORREIA, A. & RAMALHO, E. 1998. Heat flow, heat production, and lithospheric thermal regimen in the Iberian Peninsula. *Tectonophysics*, **291**, 29–53.

FOLEY, S. F., JACKSON, S. E., FRYER, B. J., GREENOUGH, J. D. & JENNER, G. A. 1996. Trace element partition coefficients for clinopyroxene and phlogopite in an alkaline lamprophyre from Newfounland by LA-ICP-MS. *Geochimica et Cosmochimica Acta*, **60**, 629–638.

FREY, F. A., SUEN, C. J. & STOCKMAN, H. W. 1985. The Ronda high temperature peridotite: geochemical and petrogenesis. *Geochimica et Cosmochimica Acta*, **49**, 2469–2491.

GALÁN, G., OLIVERAS, V. & PATERSON, B. A. 2008. Types of metasomatism in mantle xenoliths enclosed in Neogene–Qaternary alkaline mafic lavas from Catalonia (NE Spain). *In*: COLTORTI, M. & GRÉGOIRE, M. (eds) *Metasomatism in Oceanic and Continental Lithospheric Mantle*. Geological Society, London, Special Publications, **293**, 121–153.

GRANET, M., WILSON, M. & ACHAUER, U. 1995. Imaging a mantle plume beneath the French Massif Central. *Earth Planetary Science Letters*, **136**, 281–296.

HART, S. R. & DUNN, T. 1993. Experimental cpx/melt partitioning of 24 trace element. *Contributions to Mineralogy and Petrology*, **113**, 1–8.

HAURI, E. H., SHIMIZU, N., DIEU, J. J. & HART, S. R. 1993. Evidence for hotspot-related carbonatite metasomatism in the oceanic upper mantle. *Nature*, **365**, 221–227.

ISHIMARU, S. & ARAI, S. 2009. Highly silicic glasses in peridotite xenoliths from Avacha volcano, Kamchatka arc; implications for melting and metasomatism within sub-arc mantle. *Lithos*, **107**, 93–106.

ISMAIL, M., DELPECH, G., COTTIN, J. Y., GRÉGOIRE, M., MOINE, B. N. & BILAL, A. 2008. Petrological and geochemical constraints on the composition of the lithospheric mantle beneath the Syrian rift, northern part of the Arabian plate. *In*: COLTORTI, M. & GRÉGOIRE, M. (eds) *Metasomatism in Oceanic and Continental Lithospheric Mantle*. Geological Society, London, Special Publications, **293**, 223–251.

IONOV, D. A., CHANEFO, I. & BODINIER, J.-L. 2005. Origin of Fe-rich lherzolites and wehrlites from Tok, SE Siberia by reactive melt percolation in refractory mantle peridotites. *Contributions to Mineralogy and Petrology*, **150**, 335–353.

LA TOURRETTE, T., HERVIG, R. L. & HOLLOWAY, J. R. 1995. Trace element partitioning between amphibole, phlogopite, and basanite melt. *Earth Planetary Science Letters*, **135**, 13–30.

LE BAS, M. J., LE MAITRE, R. W., STRECKEISEN, A. & ZANETIN, B. A. 1986. Chemical classification of volcanic rocks based in the total alkali-silica diagram. *Journal of Petrology*, **27**, 745–750.

LÓPEZ-RUIZ, J., CEBRIÁ, J. M. & DOBLAS, M. 2002. Cenozoic volcanism I: the Iberian peninsula. *In*: GIBBONS, W. & MORENO, T. (eds) *The Geology of Spain*. Geological Society, London, 417–438.

LÓPEZ-RUIZ, J., CEBRIÁ, J. M., DOBLAS, M., OYARZUN, R., HOYOS, M. & MARTÍN, C. 1993. The late Cenozoic alkaline volcanism of the central Iberian Peninsula (Calatrava Volcanic Province, Spain): intraplate volcanism realted to extensional tectonics. *Journal of the Geological Society, London*, **150**, 915–922.

LUSTRINO, M. & WILSON, M. 2007. The circum-Mediterranean anorogenic Cenozoic igneous province. *Earth Science Reviews*, **81**, 1–65.

MCDONOUGH, W. F. & SUN, S. 1995. The composition of the Earth. *Chemical Geology*, **120**, 223–253.

NIMIS, P. & ULMER, P. 1998. Clinopyroxene geobarometry of magmatic rocks Part 1: an expanded structural geobarometer for anhydrous and hydrous, basic and ultrabasic systems. *Contributions to Mineralogy and Petrology*, **133**, 122–135.

NIU, Y. 1997. Mantle melting and melt extraction processes beneath ocena ridges: evidence from abyssal peridotites. *Journal of Petrology*, **38**, 1047–1074.

NIXON, P. H. 1987. *Mantle Xenoliths*. Wiley, Chichester.

NORMAN, M. D. 1998. Melting and metasomatism in the continental lithosphere: laser ablation ICPMS anlysis of minerals in spinel lherzolites from eastern Australia. *Contributions to Mineralogy and Petrology*, **130**, 240–255.

OREJANA, D., VILLASECA, C. & PATERSON, B. A. 2006. Geochemistry of pyroxenitic and hornblenditic xenoliths in alkaline lamprophyres from the Spanish Central System. *Lithos*, **86**, 167–196.

OREJANA, D. & VILLASECA, C. 2008. Heterogeneous metasomatism in cumulate xenoliths from the Spanish Central System: implications for percolative fractional crystallization of lamprophyric melts.

In: COLTORTI, M. & GRÉGOIRE, M. (eds) *Metasomatism in Oceanic and Continental Lithospheric Mantle*. Geological Society, London, Special Publications, **293**, 101–120.

OSSAN, A. 1889. Beitrage zur kemntniss der eruptivegesteine des Capo de Gata (Almería). *Zeitschrift der Deutschen Geologischen Gesellschaft*, **51**, 306–311.

PEARCE, J. A., BARKER, P. F., EDWARDS, S. J., PARKINSON, I. J. & LEAT, P. T. 2000. Geochemistry and tectonic significance of peridotites from the South Sandwich arc-basin systems, south Atlantic. *Contributions to Mineralogy and Petrology*, **139**, 36–53.

PEARSON, D. G., CANIL, D. & SHIREY, S. B. 2005. Mantle samples included in volcanic rocks: xenoliths and diamonds. *In*: CARLSON, R. W. (ed.) *The Mantle and Core. Treatise on Geochemistry*, **2**, 171–275.

PERINELLI, C., ORLANDO, A., CONTE, A. M., ARMIENTI, P., BORRINI, D., FACCINI, B. & MISITI, V. 2008*a*. Metasomatism induced by alkaline magma in the upper mantle of northern Victoria Land (Antarctica): an experimental approach. *In*: COLTORTI, M. & GRÉGOIRE, M. (eds) *Metasomatism in Oceanic and Continental Lithospheric Mantle*. Geological Society, London, Special Publications, **293**, 279–302.

PERINELLI, C., SAPIENZA, G. T., ARMIENTI, P. & MORTEN, L. 2008*b*. Metasomatism of the upper mantle beneath the Hyblean Plateau (Sicily): evidence from pyroxenes and glass in peridotite xenoliths. *In*: COLTORTI, M. & GRÉGOIRE, M. (eds) *Metasomatism in Oceanic and Continental Lithospheric Mantle*. Geological Society, London, Special Publications, **293**, 197–221.

PIROMALLO, C., GASPERINI, D., MACERA, P. & FACCENNA, C. 2008. A late-Cretaceous contamination episode of the European–Mediterranean mantle. *Earth and Planetary Science Letters*, **268**, 15–27.

PRELEVIC, D., FOLEY, S. F., ROMER, R. & CONTICELLI, S. 2008. Mediterranean tertiary lamproites derived from multiple source components in postcollisional geodynamics. *Geochimica et Cosmochima Acta*, **72**, 2125–2156.

REYES, J., VILLASECA, C., BARBERO, L., QUEJIDO, A. J. & SANTOS, J. F. 1997. Descripción de un método de separación de Rb, Sr, Sm y Nd en rocas silicatadas para estudios isotópicos. *Congreso Ibérico de Geoquímica*, **I**, 46–55.

SAN MIGUEL DE LA CÁMARA, M. 1936. *Estudio de las rocas eruptivas de España*. Memoria Academia de Ciencias de Madrid (Ciencias Naturales), **6**.

SEGHEDI, I., BRÄNDLE, J. L., SZAKÁCS, A., ANCOCHEA, E. & VASELLI, O. 2002. El manto litosférico en el sureste de España: Aportaciones de los xenolitos englobados en rocas alcalinas del Mioceno-Plioceno. *Geogaceta*, **32**, 27–30.

SHAW, C. S. J. & DINGWELL, D. B. 2008. Experimental peridotite–melt reaction at one atmosphere: a textural and chemical study. *Contributions to Mineralogy and Petrology*, **155**, 199–214.

SHIMIZU, Y., ARAI, S., MORISHITA, T., YURIMOTO, H. & GERVILLA, F. 2004. Petrochemical characteristics of felsic veins in mantle xenoliths from Tallante (SE Spain): an insight into activity of silicic melt within the mantle wedge. *Transactions of the Royal Society of Edinburgh: Earth Sciences*, **95**, 265–276.

TAKAZAWA, E., FREY, F. A., SHIMIZU, N. & OBATA, M. 2000. Whole rock compositional variations in an upper mantle peridotite (Horman, Hokkaido, Japan): Are they consistent with a partial melting process? *Geochimica et Cosmochimica Acta*, **64**, 695–716.

TOURON, S., RENAC, C., O'REILLY, S. Y., COTTIN, J. Y. & GRIFFIN, W. L. 2008. Characterization of the metasomatic agent in mantle xenoliths from Devès, Massif Central (France) using coupled *in situ* trace-element and O, Sr and Nd isotopic compositions. *In*: COLTORTI, M. & GRÉGOIRE, M. (eds) *Metasomatism in Oceanic and Continental Lithospheric Mantle*. Geological Society, London, Special Publications, **293**, 177–196.

UYSAL, I., KALIWODA, M., KARSLI, O., TARKIAN, M., SADIKLAR, M. B. & OTTLEY, C. J. 2007. Compositional variations as a result of partial melting and melt–peridotite interaction in an upper mantle section from the Ortaca area, SW Turkey. *Canadian Mineralogist*, **45**, 1471–1493.

VILLASECA, C., OREJANA, D., PATERSON, B. A., BILLSTROM, K. & PÉREZ-SOBA, C. 2007. Metaluminous pyroxene-bearing granulite xenoliths from the lower continental crust in central Spain: their role in the genesis of Hercynian I-type granites. *European Journal of Mineralogy*, **19**, 463–477.

WITT-EICKSCHEN, G. & KRAMM, U. 1997. Mantle upwelling and metasomatism beneath central Europe: geochemical and isotopic constraints from mantle xenolithsfrom the Rhön (Germany). *Journal of Petrology*, **38**, 479–493.

WOOD, B. J. & BANNO, S. 1973. Garnet–orthopyroxene and Orthopyroxene–clinopyroxene relationships in simple and complex systems. *Contributions to Mineralogy and Petrology*, **42**, 109–124.

XU, X., O'REILLY, S. Y., GRIFFIN, W. L. & ZHOU, X. 2003. Enrichment of upper mantle peridotite: petrological, trace element and isotopic evidence in xenoliths from SE China. *Chemical Geology*, **198**, 163–188.

YAXLEY, G. M. & KAMENETSKY, V. 1999. Insitu origin for glass in mantle xenoliths from southeastern Australia: insight from trace element compositions of glasses and metasomatic phases. *Earth and Planetary Science Letters*, **172**, 97–109.

YAXLEY, G. M., KAMENETSKY, V., GREEN, D. H. & FALLON, T. J. 1997. Glasses in mantle xenoliths from western Victoria, Australia, and their relevance to mantle processes. *Earth and Planetary Science Letters*, **148**, 433–446.

ZINDLER, A. & HART, S. R. 1986. Chemical geodynamics. *Annual Review of Earth and Planetary Sciences*, **14**, 493–571.